Regulation of adaptive growth decisions via phosphorylation of the TRAPPII complex in Arabidopsis.

Christian Wiese[1,2], Miriam Abele[2,3], Benjamin Al[2], Melina Altmann[4], Alexander Steiner[2], Nils Kalbfuß[2], Alexander Strohmayr[1,2], Raksha Ravikumar[2], Chan Ho Park[5], Barbara Brunschweiger[2], Chen Meng[3], Eva Facher[6], David W. Ehrhardt[5], Pascal Falter-Braun[4], Zhi-Yong Wang[5], Christina Ludwig[3] and Farhah F. Assaad[1,2,*]

[1]Biotechnology of Natural Products, TUM School of Life Sciences, Technical University of Munich, 85354 Freising, Germany.
[2]Botany, TUM School of Life Sciences, Technical University of Munich, 85354 Freising, Germany.
[3]Bavarian Center for Biomolecular Mass Spectrometry (BayBioMS), TUM School of Life Sciences, Technical University of Munich, 85354 Freising, Germany.
[4]Institute of Network Biology (INET), Helmholtz Center Munich, German Research Center for Environmental Health, 85764 Neuherberg, Germany.
[5]Department of Plant Biology, Carnegie Institution for Science, Stanford, 94305 California, USA.
[6]Systematic Botany and Mycology, Faculty of Biology, Ludwig-Maximilians-Universität (LMU) München, 82152 Planegg-Martinsried, Germany.
* Corresponding author. Email: farhah.assaad@tum.de

ABSTRACT

Plants often adapt to adverse or stress conditions via differential growth. The trans-Golgi Network (TGN) has been implicated in stress responses, but it is not clear in what capacity it mediates adaptive growth decisions. In this study, we assess the role of the TGN in stress responses by exploring the interactome of the Transport Protein Particle II (TRAPPII) complex, required for TGN structure and function. Together with yeast-two-hybrid screens, this identified shaggy-like kinases (GSK3/AtSKs) as TRAPPII interactors. Kinase assays and pharmacological inhibition provided *in vitro* and *in vivo* evidence that AtSKs target the TRAPPII-specific subunit AtTRS120. We identified three GSK3/AtSK phosphorylation sites in AtTRS120. These sites were mutated, and the resulting AtTRS120 phosphovariants subjected to a variety of single and multiple stress conditions. The non-phosphorylatable TRS120 mutant exhibited enhanced adaptation to multiple stress conditions and to osmotic stress whereas the phosphomimetic version was less resilient. This suggests that

the TRAPPII phosphostatus mediates adaptive responses to abiotic stress factors. AtSKs are multitaskers that integrate a broad range of signals. Similarly, the TRAPPII interactome is vast and considerably enriched in signaling components. An AtSK-TRAPPII interaction would integrate all levels of cellular organization and instruct the TGN, a central and highly discriminate cellular hub, as to how to mobilize and allocate resources to optimize growth and survival under limiting or adverse conditions.

Key words: TRAPPII, GSK3/shaggy-like kinases, BRASSINOSTEROID INSENSITIVE 2 (BIN2), decision-making, growth trade-offs, light responses, water stress, adaptation, osmotic stress, additive stress, TGN, Arabidopsis

INTRODUCTION

Plant responses to environmental stimuli involve diverse forms of growth or movement. The slow, cyclic movement of shoots and stems helps climbing plants such as vines find supportive structures, and stem growth or tendrils are then used to wrap around and cling to such structures (Darwin, 2009). Leaf movements linked to the circadian rhythm enable plants to maximize their exposure to sunlight (McClung, 2006). Tropisms are additional examples of movement in plants: the shoot bends towards directional light, whereas the root bends away from the light. In addition to phototropism, plants have tropic responses to a range of stimuli including moisture, fluctuations in temperature, gravity, touch and other mechanical cues (Garzón & Keijzer, 2011). Darwin argues that the movements of plants are driven by growth and the need to access resources, such as sunlight and water (Darwin, 2009). Leaf movements are driven either by specialized motor cells or by the differential expansion of cells on the adaxial and abaxial sides of petioles (Whippo & Hangarter, 2009; Polko *et al*, 2012; Rauf *et al*, 2013). Gyrations, revolutions and tropisms require some form of differential growth or bending at the organ level. Bending is achieved when one side of an organ grows more rapidly than the opposing side. This differential growth is a result, at least in part, of the differential sorting of PIN-FORMED (PIN) auxin transporters, resulting in the unequal distribution of auxin, a morphogen, at opposing sides of a cell (Friml *et al*, 2002; Ding *et al*, 2011). It follows that differential growth responses such as bending require differential sorting decisions. How environmental stimuli are translated into sorting decisions remains largely unclear.

The sorting of PIN transporters has been shown to require trans-Golgi network (TGN) function. Indeed, disruption of TGN function by mutation results in the ectopic distribution of PIN or AUX proteins (Naramoto *et al*, 2014; Qi *et al*, 2011; Rybak *et al*, 2014; Ravikumar *et al*, 2018). The TGN plays a key role not only in the sorting of macromolecules, but also in exocytosis and endocytosis. In addition, the TGN performs specialized functions such as cytokinesis, cell differentiation, the establishment of cell polarity, and anisotropic growth (Gendre *et al*, 2015; Ravikumar *et al*, 2017). As an early endosome, the plant TGN is a central hub in the flow of information to and from the plant cell surface (Uemura, 2016). The plant TGN has been implicated in responses to abiotic stimuli such as drought, heat, salt stress and osmotic stress and to biotic stimuli such as fungal attack (Rosquete & Drakakaki, 2018). Studies on the role of the TGN in stress responses have been carried out predominantly with core trafficking components such as Rab-GTPases, tethering factors, and Q-SNAREs, required for membrane tethering, docking and fusion (Rosquete & Drakakaki, 2018; Ravikumar *et al*, 2017). Trafficking mutants typically exhibit root growth defects and/or hypersensitivity to abiotic cues such as salt stress, osmotic stress, drought or heat (Asaoka *et al*, 2013; Kim & Bassham, 2011; Lee *et al*, 2006; Rosquete *et al*, 2019; Uemura *et al*, 2012; Wang *et al*, 2011; Zhu *et al*, 2002). However, whether trafficking mutants have primary defects in growth with secondary consequences in stress responses, or whether the primary defects lie in an ability to respond to stress factors remains unclear. More broadly, in the context of stress responses the question pertains as to whether the TGN is involved in decision-making processes *per se*, or merely in the execution of adaptive growth decisions.

As regards decision-making processes, there is a growing body of evidence to suggest that plants have the ability to learn, to process information, to communicate, to reach decisions, and in general to exhibit behavior that could be considered cognitive (reviewed in Severino, 2021). For instance, researchers have found that plants can "remember" a previous exposure to stress and respond more effectively to that same stressor in the future (Galviz *et al*, 2020). Plants can allocate resources such as nutrients to different parts of the plant in a way that maximizes their overall fitness (Ericsson, 1995). Plants can also reach adaptive decisions in response to their environment; for example, some plants can detect the presence of a nearby competitor and adjust their growth patterns to optimize access to resources (Silvertown & Gordon, 1989). There is still controversy in the scientific community over the appropriate use of terms to describe the above observations. Some scientists argue that the behaviors observed in plants are better explained by simpler mechanisms, such as chemical or mechanical responses, rather than true cognitive processes. To avoid such controversy, Severino (2021) makes the case for experimental

102 approaches. A recent experimental approach for the study of decision-making processes in
103 germinating seedlings has incorporated two tools used in decision theory: the use of a limited
104 budget and of conflict-of interest scenarios (Kalbfuß *et al*, 2022). A limited budget was achieved
105 by germination in the dark and a conflict-of-interest by the simultaneous withdrawal of light and
106 water; as a binary readout for responses to these additive stress conditions, tradeoffs in hypocotyl
107 versus root growth were monitored (Kalbfuß *et al*, 2022). By emphasizing growth trade-offs, the
108 experimental approach developed by Kalbfuß *et al* (2022) is aligned with the definition of decision-
109 making as entailing an appraisal of the advantages and disadvantages of various courses of action
110 (Karban & Orrock, 2018). While Kalbfuß *et al* (2022) address decision-making at a cellular level,
111 the literature on plant decision-making has, to our knowledge, not included considerations about
112 the possible role of the TGN.
113
114 In order to understand the role of the TGN in adaptive or stress responses, it would be important
115 to deploy a battery of gene products not only broadly associated with or localized to the TGN, but
116 also intrinsic to TGN structure and function. Two such proteins or complexes are ECHIDNA and
117 the Transport Protein Particle II (TRAPPII) tethering complex. ECHIDNA was identified as an
118 upregulated transcript in elongating cells (Gendre *et al*, 2011). *echidna* mutants have defects in
119 cell elongation and hook formation as well as in pollen formation, release and fertilization (Boutté
120 *et al*, 2013; Fan *et al*, 2014; Gendre *et al*, 2011, 2013; Ravikumar *et al*, 2018). The Arabidopsis
121 TRAPPII (AtTRAPPII) complex was identified by mutation in screens for seedlings with aberrant
122 morphogenesis or cytokinesis defects (Söllner *et al*, 2002; Thellmann *et al*, 2010; Jaber *et al*,
123 2010). AtTRAPPII most resembles fungal and metazoan TRAPPII complexes, with the exception
124 of one plant-specific subunit (Garcia *et al*, 2020; Kalde *et al*, 2019; Pinar *et al*, 2019). We have
125 previously shown that ECHIDNA and TRAPPII have overlapping yet distinct functions at the TGN
126 (Ravikumar *et al*, 2018). ECHIDNA is primarily required for the genesis of secretory vesicles and,
127 as a consequence, for cell expansion (Boutté *et al*, 2013; Gendre *et al*, 2013; McFarlane *et al*,
128 2013). AtTRAPPII plays a role not only in basal TGN functions - exocytosis, endocytosis, protein
129 sorting - but also in more specialized TGN functions such as cytokinesis and the establishment of
130 cell polarity (Ravikumar *et al*, 2018). Whether or not AtTRAPPII plays a role in responses to abiotic
131 cues such as osmotic or drought stress remains to be determined.
132
133 In this study, we focus on the TRAPPII complex as a starting point as it is required for all aspects
134 of TGN function, including the sorting of proteins such as PINs to distinct membrane domains (Qi
135 *et al*, 2011; Ravikumar *et al*, 2018). We first explored the TRAPPII interactome and also surveyed

136 dynamic or conditional interactions. Together with yeast-two-hybrid screens, this identified
137 shaggy-like kinases such as AtSK21/BIN2 as TRAPPII interactors. We corroborated this finding
138 with *in vitro* kinases assays and pharmacological inhibition *in vivo*. Shaggy-like kinases are multi-
139 taskers that integrate a vast number of biotic and abiotic cues (Lv & Li, 2020; Planas-Riverola *et*
140 *al*, 2019; Youn & Kim, 2015; Li *et al*, 2021; Song *et al*, 2023). AtSK21/BIN2 has recently been
141 implicated in decision-making in the Arabidopsis seedling (Kalbfuß *et al*, 2022). We explore the
142 meaning of the AtSK-TRAPPII interaction using a variety of assays to monitor stress responses
143 and differential growth decisions.
144
145
146 **RESULTS**
147 **The TRAPPII interactome contains a large number of signaling components**
148 To gain insight into TGN function, we used the TRAPPII interactome as a starting point. We have
149 previously identified TRAPP and EXOCYST subunits, cytoskeletal proteins and Rab GTPases in
150 the TRAPPII interactome (Rybak *et al*, 2014; Steiner *et al*, 2016; Kalde *et al*, 2019; Garcia *et al*,
151 2020). However, no global meta-analysis of the vast Arabidopsis TRAPPII interactome has been
152 carried out to date. We, therefore, performed a gene ontology (GO) term enrichment analysis.
153 AtTRAPPII consists of six shared core subunits and three TRAPPII-specific subunits (AtTRS120,
154 CLUB/AtTRS130 and TRIPP; Garcia *et al*, 2020; Kalde *et al*, 2019). We focused on the TRAPPII-
155 specific CLUB-GFP interactome. The TRAPPII interactome was significantly enriched in proteins
156 involved in (i) cell division, (ii) the organization of the cytoskeleton or of cellular or sub-cellular
157 compartments and (iii) in trafficking or transport (Fig. 1A). This is consistent with known *trappii*
158 phenotypes such as defects in microtubule organization, in cytokinesis and in the structure and
159 function of the TGN (Jaber *et al*, 2010; Qi *et al*, 2011; Rybak *et al*, 2014; Steiner *et al*, 2016;
160 Ravikumar *et al*, 2018). GO terms describing developmental processes were also scored, and this
161 is equally unsurprising in light of *trappii* defects in root growth, in root hair morphogenesis, in
162 transmission through the pollen and in vein development (Fig. 1A; Jaber *et al*, 2010; Naramoto *et*
163 *al*, 2014; Söllner *et al*, 2002; Thellmann *et al*, 2010). GO terms describing transcription, translation
164 and post-translational protein modifications such as deneddylation, acetylation and
165 dephosphorylation were also prominently enriched (Fig. 1A). Interestingly, a large number of
166 significantly enriched GO categories describe responses to abiotic cues such as light, cold, metal
167 ions or chemicals (grouped under “response to stimulus” in Fig. 1A).
168 To further explore a possible implication of the TRAPPII complex in signaling, we surveyed the
169 dynamic interactome, by which we refer to interactors perceived under one environmental

170 condition (for example in the light) but not in another (for example in the dark). By these criteria,
171 brassinosteroid signaling components were significantly enriched (p = 0.016); this category
172 encompasses 11 proteins, of which 9 were detected in CLUB-GFP immunoprecipitates from light-
173 grown influorescences (Fig. S1; Table S2). Among these were the TOR kinase and a family of
174 shaggy-like kinases (AtSKs; Fig. S1; Table S2). TOR and AtSKs are highly significant interactors
175 in the TRAPPII interactome (Fig. S1; Fig. 1B). They show a fold enrichment that is lower than seen
176 for components of the TRAPPII complex, but similar to that seen for validated interactors such as
177 RabA2a and MAP65, expected to form more transient associations (Fig. S1; Fig. 1B; Kalde *et al*,
178 2019; Steiner *et al*, 2016). We then used yeast two-hybrid (Y2H) to probe for binary interactions
179 between TRAPPII and signaling components identified in the IP-MS. Y2H was carried out with
180 TRAPPII subunits and truncations thereof (Kalde *et al*, 2019; Steiner *et al*, 2016; Garcia *et al*,
181 2020). In a large scale Y2H screen including 2400 pair-wise tests, an interaction was detected
182 between a TRS120$^{499-1187}$ truncation (referred to below as TRS120-T2) and the shaggy-like kinase
183 BIN2 (AtSK21; Fig. 1C). BIN2 interacted specifically with AtTRS120 and not with other tested
184 TRAPPII subunits (Fig. 1C). Furthermore, we did not detect any other TRAPPII-kinase interactions
185 in our pairwise Y2H assays.
186
187 **The TRAPPII complex is a target of shaggy-like kinases**
188 To assess whether the TRAPPII complex is a target of AtSK/GSK3 kinases, we first looked for the
189 presence of phosphopeptides in co-immunoprecipitates. To this end, we immunoprecipitated two
190 TRAPPII-specific subunits, AtTRS120 and CLUB/AtTRS130, and looked for phosphopeptides via
191 mass spectrometry. This provided ample *in vivo* evidence for TRAPPII AtTRS120 phosphorylation
192 at AtSK/GSK3 sites (Fig. S2). Furthermore, shaggy-like kinases were detected in IP-MS not only
193 with the TRAPPII-specific subunit CLUB/AtTRS130 (Fig. 1B; Fig. S1) but also with the TRAPPII-
194 specific subunit AtTRS120 (Fig. S3). The Arabidopsis genome encodes ten shaggy-like kinases
195 (AtSKs), which are classified into four clades (Fig. S3A).
196 The TRS120-T2 truncation contains the GSK3 sites we had found to be phosphorylated *in vivo*
197 (Fig. S2; see yellow highlights in Fig. 2B). Our nomenclature for these sites is α, β and γ, which is
198 short for TRS120-S922:S923 (α), TRS120-S971:S973:S974:S975 (β) and TRS120-S1165 (γ; Fig.
199 2B). Alpha-fold structural predictions (Varadi *et al*, 2022; Jumper *et al*, 2021) show that the three
200 sites reside in unstructured, flexible and accessible regions of the AtTRS120 protein, as is
201 observed in the majority of modified amino acid residues (Fig. 2C-D; Jiménez *et al*, 2007). These
202 reside in the plant-specific moiety of AtTRS120 and are embedded in plant-specific sequences at
203 the dimer interface (see green shading in Fig. 2A; Fig. 2E). To study the three sites, we generated

site directed mutations in TRS120-T2, mutating the serine (S) and threonine (T) residues (depicted in red in Fig. 2B) to non-phosphorylatable alanine (A) residues, or to aspartate (D) to mimic constitutive phosphorylation. In the case of the TRS120-Sβ site, for example, we designate these variants as TRS120-SβA or TRS120-SβD (Fig. 2F; Fig. 3A). The point mutations were introduced into cDNA sequences for expression in yeast and bacteria.

The IP-MS and Y2H interactions were validated with *in vitro* kinase assays, performed with a phosphorus radioisotope (Fig. 3A; Fig. S4). Further, the phosphorylation was confirmed with mass-spectrometry using non-radioactive assays. The mass-spectrometry results showed that the AtTRS120 α, β, and γ sites phosphorylated *in vivo* (Fig. S2; IP-MS on seedlings using TRS120-GFP as bait) were phosphorylated by AtSKs *in vitro* (Fig. 3B, 3C). Kinase assays performed with varying kinase concentrations (but constant substrate concentrations) showed that the phosphorylation events were time and/or concentration dependent (Fig. 3C). AtTRS120 was a substrate of AtSKs in clades I-III; we did not detect phosphorylation of AtTRS120 with a clade IV AtSK *in vitro* (Fig. 3C). All AtSKs that targeted AtTRS120 had a marked and consistent preference for the TRS120-γ (S1165) site (Fig. 3C). *In vivo*, IP-MS performed on seedlings treated with the AtSK inhibitor bikinin showed a reduced extent of phosphorylation of the TRS120-γ peptide (Fig. S5), which is consistent with the *in vitro* data (Fig. 3C). In Y2H screens, the BIN2-TRS120 interaction, but not TRAPPII complex interactions, was almost abolished when all three sites were mutated from S to D (TRS120-SαβγD; Fig. 2F). In summary, several lines of *in vitro* (Y2H, kinase assays) and *in vivo* (IP-MS, pharmacological inhibition) evidence support the conclusion that the TRAPPII subunit AtTRS120 is a substrate of shaggy-like kinases.

BIN2 and TRAPPII are required for differential growth decisions under additive stress

As TRAPPII is a BIN2 substrate, a question is whether *bin2* and *trappii* mutants have related phenotypes. We were not able to detect cytokinesis or protein sorting defects, characteristic of *trappii,* in semi-dominant *bin2-1* alleles (Fig. S6). We have recently shown that BIN2 is required for hypocotyl versus root tradeoffs in the germinating seedling under additive stress conditions involving the simultaneous withdrawal of both light and water (Kalbfuß *et al*, 2022). Water stress in the dark is a “conflict of interest” scenario in which hypocotyl and root growth have competing interests (Kalbfuß *et al*, 2022). Kalbfuß *et al*, 2022 defined decision mutants as ones that had either insignificant responses ($P > 0.05$), or consistently wrong growth responses as compared to the wild-type ($P < 0.05$ but for an opposite growth phenotype, as depicted by red asterisks in Fig. 4B, 4C, 4D; Kalbfuß *et al*, 2022). Under additive stress, *trappii* null mutants failed to adjust their

238 hypocotyl length along the same line as the wild-type (red asterisk in Fig. 4C, 4D; see Fig. 4F for
239 a direct comparison to the wild-type and for the distribution of datapoints). In particular, *trappii*
240 *trs120-4* mutants had non-significant hypocotyl/root ratio responses to water withdrawal in the
241 dark (Fig. 4D). Due to some variability between PEG plates and experiments, we normalized each
242 mutant line to its corresponding wild-type ecotype on the same (PEG) plate in the same
243 experiment. To this end, the response to water stress in the dark was represented as a normalized
244 response quotient (RQ). The RQ is an indication of how much the mutant deviates from the
245 corresponding wild-type and enables us to summarize replicate experiments (see methods for
246 further detail; the RQ_{ratio} is depicted in Fig. 4G and the $RQ_{hypocotyl}$ and RQ_{root} in Fig. S7). We reason
247 that mutants unable to integrate environmental cues might have a "confused phenotype" under
248 multiple stress conditions. The read out for a "confused phenotype" would translate into erratic
249 (i.e. highly variable) hypocotyl versus root lengths. This high variance would, in turn, translate into
250 a low signal-to-noise ratio, and this can be seen as a high *P*-value. We, therefore, plotted the
251 median *P*-values against the normalized response quotients (referred to as volcano plots; mean
252 RQ_{ratio} in Fig. 4H). Wild-type ecotypes invariably had low *P*-values < 10^{-10} (grey shading on the red
253 line in Fig. 4H, green arrow). Mutants with high *P*-values and low response quotients would be
254 considered "confused" and these would map in the lower left quadrant of the RQ_{ratio} volcano plot
255 (see peach shading in Fig. 4H). *bin2* higher order null alleles and *trs120-4* mutants cluster together
256 in the lower left region of the volcano plot (see peach shading in Fig. 4H); both qualify as decision
257 mutants (Fig. 4B, 4D, 4F-H; Kalbfuß *et al*, 2022).
258
259 A question that arises is whether *trappii* mutants are impaired in differential growth decisions as a
260 secondary consequence of primary defects in cytokinesis (Jaber *et al*, 2010; Rybak *et al*, 2014;
261 Thellmann *et al*, 2010). The etiolation response was severely attenuated in *trappii* mutants, but
262 nonetheless highly significant (P < 0.00001; Fig. S8C, S8D, S8F-G). Similarly, an attenuated but
263 clear etiolation response has been shown for other cytokinesis-defective mutants including *keule*
264 and *knolle* (Assaad *et al*, 2001). This shows that, despite a severe impairment in cell division,
265 cytokinesis-defective mutants are nonetheless capable of differential growth. In addition to their
266 cytokinesis defect, *trappii* mutants are impaired in TGN function (Ravikumar *et al*, 2018). We,
267 therefore, compared *trappii* mutants to *echidna* mutants, severely impaired in TGN structure and
268 function (Boutté *et al*, 2013; Gendre *et al*, 2013; McFarlane *et al*, 2013). Both *echidna* and *trappii*
269 mutants exhibited a severe impairment in root elongation in the light (Fig. S8 C-E). In contrast to
270 *trappii*, however, *echidna* mutants had highly significant responses to additive stress that
271 resembled the wild-type in all respects (Fig. 4E, 4G, 4H). The *trappii* decision phenotype was

272 shared neither by *echidna* mutants, nor by higher order null mutants impaired in the perception of
273 light or water stress (Fig. 4G, 4H). In conclusion, a comparison to other cytokinesis-defective or
274 TGN mutants suggests that neither cytokinesis defects nor TGN malfunction suffice to explain the
275 *trappii trs120-4* decision phenotype.
276 Cellular growth parameters in *trappii* were assessed by scanning electron microscopy (SEM) in
277 the hypocotyl and by confocal microscopy in root tips. In wild-type hypocotyls, both organ length
278 and cell length decrease in response to water stress in the dark (Fig. 4A; Fig. 5A). In contrast, in
279 *trappii* mutants, organ and cell length significantly increased (red asterisks in Fig. 4C, 4D and in
280 Fig. 5B, 5C highlight a phenotype consistently opposite to the wild-type). This was more
281 pronounced in *trs120-4* (1.71-fold increase; Fig. 5C) than in *club-2* (1.46-fold increase; Fig. 5B)
282 whereas the wild-type Col-0 showed a 0.55-fold decrease in cell length. In root tips, we monitored
283 meristem properties and cell length along single cortical cell files as a function of distance from
284 the quiescent center. In the wild-type, meristem size was large in the light, intermediate in the dark
285 and shortest under water stress in the dark (darkW; Fig. 6A-C). In contrast, meristem size in
286 *trs120-4* remained constant under the three environmental conditions tested (Fig. 6E-G). We have
287 recently shown that root growth in response to water stress in the dark is due to a combination of
288 cell division and rapid exit from the meristem (Kalbfuß *et al*, 2022). An early exit from the meristem
289 can be visualized as cell elongation in cells close to the quiescent center. This was observed
290 under dark and darkW conditions in the wild-type (green arrows in Fig. 6D) but not in the *trappii*
291 mutant *trs120-4* (magenta arrows in Fig. 6H). While the curves differed under the different
292 environmental conditions in the wild-type (Fig. 6D), these were fairly similar regardless of the
293 environmental cue in *trs120-4* (magenta arrows in Fig. 6H; note that the grey shading, which
294 designates the 95% confidence interval, overlaps). We conclude that, at a cellular level, *trappii*
295 *trs120-4* mutants are unable to differentially regulate their growth parameters (Fig. 5, Fig. 6). This
296 would suffice to explain the growth defects we observed at the organ level (Fig. 4). In summary,
297 *bin2* and *trappii* alleles have related phenotypes w.r.t. an inability to differentially regulate cell
298 growth in both the hypocotyl and root tip in response to additive stress (Figs. 4-6; cf. Kalbfuß *et*
299 *al*, 2022).
300
301 **AtTRS120 phosphovariants are functional**
302 To assess the impact of phosphorylation status on intracellular localization, targeted point
303 mutations at the TRS120 AtSK sites (Fig. 2B) were introduced into genomic sequences capable
304 of rescuing the *trs120-4* mutant phenotype (Rybak *et al*, 2014). The TRS120 constructs were
305 fused to a C-terminal GFP tag and we refer to the ensuing site-directed mutants as TRS120

306 phosphovariants. The constructs were expressed and capable of rescuing the null *trs120-4* allele
307 in the T1 and T2 generations (Fig. S9A, S9B); upon further propagation, however, the GFP signal
308 (but not the ability to rescue the mutant phenotype) was lost and signs of silencing were evident
309 (Fig. S9C, S9D). The wild-type TRAPPII complex resides in the cytosol, at the TGN and at the cell
310 plate (Fig. S10A; Naramoto *et al*, 2014; Qi *et al*, 2011; Ravikumar *et al*, 2018; Rybak *et al*, 2014).
311 Phosphovariants had a similar appearance, but the phosphomimetic S to D variant tended to be
312 mostly membrane associated, with almost no detectable cytosolic signal (Fig. S10).
313

314 **TRS120-SαβγA and TRS120-SαβγD have opposite effects on seed germination under**
315 **osmotic stress**

316 We first analyzed the impact of osmotic stress on the germination frequencies of TRS120
317 phosphovariants. Different TRS120-SαβγA and TRS120-SαβγD primary transformants were
318 plated on media containing 0, 200, or 400 mM mannitol (Fig. 7A-C). As compared with the control
319 (Col-0), the TRS120-SαβγA phosphovariant had higher seed germination rates on mannitol: on
320 day 4 we observed 70% germination in TRS120-SαβγA versus 35% germination for the control
321 on 400 mM mannitol as an osmotic agent (Fig. 7C). In this respect, TRS120-SαβγA was similar to
322 the ABA deficient mutant *aba2-1* on mannitol (Fig. 7C). In contrast, the TRS120-SαβγD
323 phosphovariant exhibited delayed and reduced germination, with lower maximal germination
324 rates, even in the absence of mannitol (Fig. 7A-C). Indeed, on 400 mM mannitol TRS120-SαβγD
325 mutants reached a maximal germination rate of 60% compared to 90% for the wild-type. With
326 respect to its delay in germination, TRS120-SαβγD was similar to the ABA coreceptor higher order
327 mutant *hab1-1 abi1-2 pp2ca-1* on mannitol (Fig. 7C). In summary, the non-phosphorylatable
328 TRS120-SαβγA mutations enhanced whereas the phosphomimetic TRS120-SαβγD mutations
329 reduced germination on mannitol.
330

331 **TRS120 phosphorylation status affects hypocotyl versus root trade-offs under additive**
332 **stress conditions**

333 In light of the decision phenotypes of *bin2* and *trappii* mutants and of the observation that AtSKs
334 such as BIN2 target TRAPPII, the question arises as to whether shaggy-like kinases regulate
335 differential growth decisions via TRS120 phosphorylation. To test this hypothesis, AtTRS120
336 phosphovariants homozygous for the null *trs120-4* allele and hemizygous for the phosphovariant
337 construct were studied under different environmental or stress conditions. The etiolation response
338 was not impacted by the phosphorylation status of AtTRS120 (Fig. S11). In contrast, TRS120
339 phosphomutants had phenotypes under additive stress conditions (Fig. 7D-F; Fig. S12). TRS120-

340 SαβγA non-phosphorylatable variants exhibited an enhanced root response under darkW
341 conditions (Fig. 7E) and a strongly enhanced ratio response to water stress in the dark (mean
342 RQ_{ratio} = 1.49; Fig. 7F). Conversely, the phosphomimetic TRS120-SαβγD mutants exhibited
343 severely attenuated responses to water stress in the dark in all respects (Fig. 7D-F; mean
344 $RQ_{hypocotyl}$= 0.66; mean RQ_{root} = 1.48; mean RQ_{ratio} = 0.44). Thus, the non-phosphorylatable
345 TRS120-SαβγA and the phosphomimetic TRS120-SαβγD mutations had opposite effects on
346 hypocotyl versus root lengths under water stress in the dark, with TRS120-SαβγA exhibiting an
347 enhanced and TRS120-SαβγD an attenuated ratio response (Fig. 7F). Under all environmental
348 conditions, the total seedling length of the phosphovariants did not significantly differ from that of
349 the wild-type AtTRS120 construct (Fig. S12D), which highlights the absence of a growth defect.
350 We conclude that the TRS120 phosphorylation status impacts the seedling's ability to differentially
351 regulate its hypocotyl and root lengths in response to additive stress conditions. Taken together,
352 the data show opposite impacts of non-phosphorylatable versus phosphomimetic mutations at
353 AtTRS120 AtSK sites in terms of (i) seed germination under osmotic stress and (ii) responses to
354 additive stress. This suggests that TRAPPII phosphorylation by shaggy-like kinases mediates
355 adaptive responses to osmotic stress and to light and water availability.
356
357
358 **DISCUSSION**
359 In this study, we explore the role of the TGN in stress responses in Arabidopsis. Our point of entry
360 is the TRAPPII complex, which has been shown to be required for TGN structure and function (Qi
361 *et al*, 2011; Ravikumar *et al*, 2018). We performed proteomic and yeast two-hybrid screens and
362 present several lines of *in vitro* (Y2H, kinase assays) and *in vivo* (IP-MS, pharmacological
363 inhibition) evidence that the TRAPPII subunit AtTRS120 is the target of AtSK kinases, including
364 BIN2. We document differential phosphorylation of three distinct AtSK/GSK3 sites by three of the
365 four AtSK clades. The phosphorylation status of AtTRS120 impacted seed germination under
366 osmotic stress as well as adaptive responses to additive stress. We show that *bin2* and *trappii*
367 alleles have related phenotypes with respect to an impaired adaptation to additive stress
368 conditions, in this instance achieved by the simultaneous withdrawal of light and water.
369 A concern when assessing the role of the TGN in stress responses is that TGN-related mutants
370 typically have pleiotropic phenotypes as a consequence of their impairment in fundamental
371 processes such as secretion, endocytosis or sorting (Rosquete & Drakakaki, 2018; Ravikumar *et*
372 *al*, 2018). To distinguish between primary defects in growth on the one hand and adaptive
373 responses on the other, we monitored trade-offs between hypocotyl and root growth under additive

374 stress conditions (Kalbfuß *et al*, 2022). We focus on *echidna* and *trappii* mutants as these have
375 been shown to impact both the structure and the function of the TGN (Boutté *et al*, 2013; Gendre
376 *et al*, 2011, 2013; McFarlane *et al*, 2013; Qi *et al*, 2011; Ravikumar *et al*, 2018). These TGN
377 mutants had hypocotyl and root growth defects, which are characteristic of trafficking mutants (Fig.
378 S8). In addition to their growth defects, *trappii trs120-4* mutants had a significant hypocotyl
379 response but in the wrong orientation as compared to the wild-type (denoted by red asterisks in
380 Fig. 4 and Fig. 5) as well as an insignificant hypocotyl/root ratio response to light and water
381 deprivation (Fig. 4). The *trappii* phenotypes described in this study are difficult to explain as mere
382 growth defects. Rather, the inability to mediate trade-offs in growth in response to additive stress
383 provides a compelling argument for TRAPPII as having a role in adaptive growth decisions.
384 Conceptually, the optimization of hypocotyl-to-root ratios can be deconstructed into four distinct
385 stages: (i) perception, (ii) signal integration, (iii) decision making and (iv) the implementation of
386 resulting actions (Kalbfuß *et al*, 2022). To address the first stage, perception, we looked at
387 quadruple *phyA phyB cry1 cry2* photoreceptor mutants; these failed to adjust their organ lengths
388 to light versus dark conditions but had a highly significant response to additive stress (Fig. 4G-H;
389 Fig. S8G-I; Kalbfuß *et al*, 2022). The opposite was true for *bin2-3 bil1 bil2* and *trappii* mutants,
390 which were able to respond to single stress factors but not to additive stress (Fig. 4; Kalbfuß *et al*,
391 2022). Shaggy-like kinases integrate a vast number of signaling pathways (Lv & Li, 2020; Youn &
392 Kim, 2015; Li *et al*, 2021; Song *et al*, 2023; Planas-Riverola *et al*, 2019). Accordingly, we have
393 postulated that the *bin2-3 bil1 bil2* „decision“ phenotype under conflict-of-interest scenarios is
394 primarily due to signal integration (Kalbfuß *et al*, 2022). Prime candidates for the fourth stage,
395 execution or implementation of the action, are *echidna* mutants; these had highly significant
396 adaptive responses - in the correct orientation - despite their growth defects (Fig. 4). The question
397 arises as to how to categorize *trappii* mutants in the above conceptual framework. Despite having
398 abnormally short hypocotyls or roots, *trappii* mutants still exhibited differential length increase
399 depending on light availability (Fig. S8). This shows that they are able to perceive and respond to
400 light.
401 If TRAPPII is primarily involved neither in perception nor in execution, this would place it at the
402 signal integration and/or decision-making steps of adaptive growth decisions. The TRAPPII
403 interactome is vast and complex, with - in addition to the expected ontologies describing traffic,
404 transport and cellular organization - a surprising number of signaling components implicated in
405 responses to abiotic cues (Fig. 1A). This suggests a role for TRAPPII in signal integration. A recent
406 study of the BIN2 signaling network describes the expected components of hormone signaling,
407 phototropism and stress responses; surprisingly, the BIN2 signaling network also includes

408 secretion, endocytosis, autophagy, TGN, endoplasmic reticulum (ER), cell wall and cytoskeleton
409 (Kim *et al*, 2023). Thus, there is a considerable compartmental overlap between the BIN2 network
410 and the TRAPPII interactome. Nonetheless, TRAPPII did not feature among the 482 members of
411 the BIN2 signaling network identified by proximity labeling (Kim *et al*, 2023). The discrepancy
412 could be due to the different methods used: yeast two hybrid and proteomics in this study versus
413 proximity labelling and phosphoproteomics in Kim *et al*, 2023. However, a multiomics approach
414 identified AtTRS120-S971 (encompassed by our identified β site AtTRS120-
415 S971:S973:S974:S975) as being differentially phosphorylated in response to brassinolide
416 treatment (Clark *et al*, 2021). This provides an additional line of *in vivo* evidence for a BIN2-
417 AtTRS120 interaction and suggests that TRAPPII phosphorylation is brassinosteroid-regulated, at
418 least for the AtTRS120-S971 residue.
419 BIN2 is a negative regulator of BR signaling and AtSK11 and AtSK12 have been shown to
420 negatively regulate root growth responses under osmotic stress (Dong *et al*, 2020; Li *et al*, 2021;
421 Song *et al*, 2023). To explore the biological significance of the AtSK-TRAPPII interaction, we
422 probed the phenotypes of TRAPPII phosphovariants. We found that these had an impact on
423 hypocotyl versus root growth tradeoffs in response to additive stress. Furthermore, the non-
424 phosphorylatable TRS120-SαβγA variant had an enhanced root adaptation whereas the
425 phosphomimetic variant decreased root growth under additive stress, which is consistent with the
426 negative regulation of growth by BIN2 and other AtSKs. We have previously described plant-
427 specific domains or subunits predicted to be at the dimer interface of the Arabidopsis TRAPPII
428 complex (marked in green in Fig. 2E; Garcia *et al*, 2020; Kalde *et al*, 2019). Interestingly, BIN2
429 interacts with the plant-specific C-terminal domain of AtTRS120, while MAP65-3 interacts with
430 plant-specific C-terminal domains of the TRAPPII-specific subunits CLUB and AtTRS120 (Steiner
431 *et al*, 2016). This presents intriguing implications regarding the potential role of the AtSK-TRAPPII
432 module in meeting the unique demands of endomembrane traffic in plants.
433 The observation that the *trappii* "decision" phenotype was not shared by *echidna* mutants raises
434 the question as to what facet of TGN function is required for responses to additive stress.
435 ECHIDNA and TRAPPII have been shown to have overlapping roles in basal TGN functions such
436 as secretion (Ravikumar *et al*, 2018). In addition, ECHIDNA regulates ER stress and immunity
437 whereas TRAPPII has roles in cytokinesis and in the establishment of cell polarity that appear to
438 be independent of ECHIDNA (Liu *et al*, 2023; Ravikumar *et al*, 2018). In the literature, there are
439 few examples of null mutants that are associated with the TGN and that have a positive influence
440 on growth. One such example is ZmBet5L1 (Zhao *et al*, 2023), which encodes a core subunit of
441 the TRAPPII complex (Kalde *et al*, 2019; Thellmann *et al*, 2010). Null alleles of ZmBet5L1 enhance

442 root growth also in the absence of stress (Zhao *et al*, 2023). The TRAPPII complex has two distinct
443 molecular functions: it acts as a tethering complex and as a Rab-GTPase guanine nucleotide
444 exchange factor (Rab-GEF). Rab-GEFs act as central cellular switches that turn GDP-bound
445 inactive Rab-GTPases to active GTP-bound forms (Elliott *et al*, 2020). Rab-GTPase cascades are
446 crucial for the development of polarity and directional growth in plants and play a vital role in
447 facilitating physiologically dynamic functions (Elliott *et al*, 2020). AtTRAPPII is thought to be a GEF
448 for the TGN-associated RabA-GTPases, a highly expanded class with 26 members (Kalde *et al*,
449 2019; Elliott *et al*, 2020). The TRAPPII interactome contains not only Rabs in the A class, but also
450 other classes of Rab GTPases such as RabF1, which is involved in stress responses (Yin *et al*,
451 2017). In contrast to ECHIDNA, which is required for the biogenesis of secretory vesicles and for
452 growth generically, as a putative Rab-A GEF TRAPPII has an ability to mediate all the highly
453 diverse facets of TGN function. In a judgement-decision model for plant behavior, judgment is a
454 composite of discrimination, assessment, recognition, and categorization (Karban & Orrock,
455 2018). In this context, it is interesting that the most expanded Rab GTPase family is TGN-
456 associated, suggestive of a tremendous degree of discrimination, specialization and
457 subcompartmentalization at the TGN.
458 Our study highlights the possible relevance of the AtSKs-TRAPPII interaction for adaptive growth
459 decisions (Fig. 8). Shaggy-like kinases such as BIN2 integrate a vast number of signaling
460 pathways and, together with receptor complexes at the cell surface, comprise a surveillance
461 system fine-tuned to both biotic and abiotic cues (Lv & Li, 2020; Planas-Riverola *et al*, 2019; Youn
462 & Kim, 2015; Li *et al*, 2021; Song *et al*, 2023). Via the cytosol, the AtSKs would then transmit this
463 information by mediating the phosphorylation status of the TRAPPII complex. TRAPPII would, in
464 turn, mediate TGN function. As an early endosome, the TGN is a central hub in the flow of
465 information to and from the cell surface. It is also intimately connected to the late endosome (or
466 the pre-vacuolar compartment) and to the Golgi, which provides complex polysaccharides as
467 building blocks for the deposition of new cell wall. Thus, the AtSK-TRAPPII interaction would
468 integrate all levels of cellular organization. We posit that signal integration and decision-making
469 occur at the AtSK-TRAPPII interface and that, downstream of TRAPPII, Rab GTPase cascades
470 are implicated in implementing decisions reached at the AtSK-TRAPPII module (Fig. 8). Sorting
471 and trafficking decisions at the TGN would enable plants to respond to developmental or
472 environmental signals via differential growth or various forms of movement.
473 Plants exhibit plasticity in their growth, meaning they can adjust their growth patterns in response
474 to environmental cues such as light, temperature, and nutrient availability. It has been argued that
475 plant phenotypic plasticity “is the result of signal integration - a process that requires cell-cell

476 communication, and that results in adaptive forms of movement not to be interpreted as automatic
477 and programmed" (Garzón & Keijzer, 2011). Movement in plants involving organ bending require
478 the polar distribution of morphogens such as auxin. This, in turn, requires the polarized localization
479 of auxin transporters such as PINs. The Arabidopsis TRAPPII complex has been shown to play a
480 pivotal role in a variety of sorting decisions including the polar localization of PIN2 proteins (Qi *et*
481 *al*, 2011; Rybak *et al*, 2014; Ravikumar *et al*, 2018). How environmental or developmental cues
482 regulate the cargo composition and sorting of TGN vesicles remains unclear. Future experiments
483 will explore the impact of the TRAPPII phosphorylation status on protein sorting, cell polarity, and
484 on the Rab specificity of TRAPPII as a putative GEF. The presence of the TOR kinase in the
485 TRAPPII interactome is intriguing, as TOR integrates information about nutrient and energy
486 availability, and has recently been shown to regulate actin dynamics as a function of ATP levels
487 (Dai *et al*, 2022); it is tempting to speculate that TOR could provide information on nutrient and
488 energy levels to the AtSK-TRAPPII "decision" module. In plants, the Trans-Golgi Network (TGN)
489 plays a critical role in the relay of information between the cell surface and intracellular
490 compartments. An AtSK-TRAPPII interaction would instruct the TGN, a central and highly
491 discriminate cellular hub, as to how to mobilize and allocate resources to optimize survival under
492 limiting or adverse conditions.
493

494 **EXPERIMENTAL PROCEDURES**
495
496 **Lines and growth conditions**
497 All the lines used in this study are listed in Table S1. Seedling-lethal mutants were propagated as
498 hetero- or hemi-zygotes. Insertion lines were selected via the TAIR and NASC web sites
499 (Swarbreck *et al*, 2008). Plants were grown in the greenhouse under controlled temperature
500 conditions and with supplemental light, or under controlled growth chamber conditions at the
501 TUMmesa ecotron (16/8 h photoperiod at 180 µmol $m^{-2}s^{-1}$). Seed were surface sterilized, stratified
502 at 4˚C for two days and plated on ½ MS medium supplemented with 1% sucrose and B5 Vitamins
503 (Sigma; https://www.sigmaaldrich.com). Plates were incubated at 22°C in constant light (80 µmol
504 $m^{-2}s^{-1}$). The root tips of five-day-old plate-grown seedlings were used for confocal microscopy.
505 Seven-day-old plate-grown seedlings were used for co-immunoprecipitation.
506
507 **Co-immunoprecipitation (IP)**
508 For CLUB/AtTRS130:GFP we used 3 g of inflorescences per IP experiment. For TRS120-GFP, 3
509 g of light-grown seedlings were harvested at day 7. For bikinin treatment, seedlings were treated
510 for 30 min with 25 µM bikinin at day 7; mock treatments were conducted in parallel.
511 Co-immunoprecipitation experiments were carried out as described previously (Rybak *et al*, 2014).
512 Briefly, seedling lysates were incubated with GFP-trap beads (Chromotek). After washing away
513 all non-binding proteins, 70 µl 2x NuPAGE LDS + 25 mM dithiothreitol (DTT) buffer (ThermoFisher,
514 US) was added and boiled at 70°C for 10 min to denature the bait and all interaction partners.
515 In-gel trypsin digestion was performed according to standard procedures (Shevchenko *et al*,
516 2006). Briefly, the samples were run on a NuPAGE 4-12% Bis-Tris Protein Gel (Thermofisher
517 Scientific, US) for 3 min. Subsequently, the still not size-separated single protein band per sample
518 was cut out of the gel, reduced (50 mM DTT), alkylated (55 mM chloroacetamide) and digested
519 overnight with trypsin (trypsin-gold, Promega). The resulting peptides were analysed by mass
520 spectrometry. More detailed information on the mass-spectrometric data acquisition is provided in
521 the supporting method section. See data deposition for access to the raw data.
522
523 **Molecular techniques and site directed mutagenesis (SDM)**
524 For subcloning for expression in *E.coli* or yeast, we used cDNA clones developed by the plant
525 genome project of RIKEN Genomic Sciences Center (Seki *et al*, 1998, 2002). Non-
526 phosphorylatable and phosphomimetic TRS120 phosphosite variant constructs (SαA, SβA, SγA,
527 SαβA, SαγA, SβγA, SαβγA and SαD, SβD, SγD, SαβD, SαβγD)) were generated using the
528 GATEWAY® cloning system and site-specific primers (see supplementary methods for substituted
529 amino acids and used primers). TRS120-T2 cDNA sequences (spanning amino acids 499-1187;
530 Rybak *et al*, 2014) were used as SDM template for protein expression in *Escherichia coli* (*E. coli*;
531 kinase assays) and in yeast (Y2H). For *in planta* experiments (confocal microscopy, IP-MS), the
532 genomic construct P_{TRS120}::TRS120-GFP (Rybak *et al*, 2014) was used as an SDM template.
533 TRS120 phosphovariants were introduced into plants via *Agrobacterium* mediated transformation
534 (see supplementary methods for further details).
535
536

537 **Yeast two-hybrid (Y2H)**
538 Y2H pairwise tests were performed as described in Altmann *et al*, 2018. Briefly, open reading
539 frames (ORFs) encoding CLUB/AtTRS130 truncations (C2, C3), TRS120 truncations (T1, T3) and
540 BIN2 were transferred by Gateway cloning into the GAL4 DNA-binding domain (DB) encoding
541 Y2H vector pDEST-pPC97, and subsequently transformed into the yeast strain Y8930. These
542 constructs were screened by yeast mating against a TRS120-T2 truncation and its
543 phosphomutants TRS120-T2- SαD, SβD, SγD, SαβD and SαβγD fused to the Gal4 activation
544 domain (AD) in the yeast strain Y8800. Interaction was assayed by growth on selective plates
545 using the *HIS3* reporter, and using 1 mM 3-Amino-1,2,4-triazole (3-AT) to suppress background
546 growth. All candidate interactions were verified by pairwise one-on-one mating in four independent
547 experiments. Only pairs scoring positives in all four assays were considered as *bona fide*
548 interaction partners.
549
550 ***In vitro* kinase assays**
551 Glutathione S-transferase (GST)-BIN2 (Li & Nam, 2002) and GST-T2-TRS120 phosphovariants
552 were expressed in *Escherichia coli* (Rosetta-gami^{TM} strain) under constant shaking for 20 h at
553 25°C or 20 h at 18°C, respectively. The expressed proteins were affinity purified with GST-tags.
554 After sonication of the samples in 1x PBS, 1 mM PMSF, 1 mg/ml lysozyme and 1% Triton X-100,
555 the bacterial cell rests were centrifuged for 30 min at 16,000 g. Supernatants were incubated for
556 2 h with Glutathione Sepharose® 4 Fast Flow Beads (GE Healthcare) while rotating. After washing
557 the samples five times, the GST tagged proteins were eluted with 10 mM glutathione and
558 concentrated by ultra-filtration.
559 *In vitro* kinase assays with radiograph readout were performed as described previously (Kim *et al*,
560 2012), with some adaptations. In short, ca. 0.1 µg GST-BIN2 and ca. 0.5 µg of a GST-T2-TRS120
561 phosphovariant were incubated in 20 mM Tris pH 7.5, 1 mM $MgCl_2$, 100 mM NaCl, 1 mM DTT,
562 100 µM ATP and 10 µCi ATP[γ-^{32}P] for 3 h at 22°C in motion. The kinase reaction was stopped
563 by adding 2x SDS sample buffer and by boiling the samples for 10 min. Protein phosphorylation
564 was analyzed by autoradiographs and SDS-PAGE.
565 *In vitro* kinase assays with mass-spectrometry readout were performed to determine specific
566 phosphorylation sites. For each reaction, 10 µg of substrate (TRS120-T2) and different dilutions
567 of the kinase (1:5, 1:10, 1:100) were incubated for 15, 30, and 120 min in a kinase buffer (20 mM
568 Tris HCl, 100 mM NaCl, 1 mM $MgCl_2$, 1 mM DTT, 1 mM ATP). For the negative controls, one
569 sample with the highest kinase concentration and the longest incubation time was incubated in a
570 kinase buffer without ATP. For the kinase dead control, the kinase was heat-inactivated prior to
571 the incubation with its substrate. To stop the reaction, samples were heated at 95°C for 5 min.
572 After reduction (10 mM DTT), alkylation (55 mM CAA) and protein digestion (trypsin-gold,
573 Promega) the resulting peptides were purified using self-packed StageTips (C18 material, 3M
574 Empore) and analyzed by mass spectrometry. More detailed information can be found in the
575 supporting methods.
576
577 **LC-MS/MS data acquisition and analysis**
578 Generated peptides were analyzed on a Dionex Ultimate 3000 RSLCnano system coupled to a
579 Q-Exactive HF-X mass spectrometer (Thermo Fisher Scientific) in data-dependent acquisition
580 mode. Peptide identification and quantification was performed using the software MaxQuant

581 (version 1.6.1.0) (Cox & Mann, 2008; Tyanova *et al*, 2016a) with its built-in search engine
582 Andromeda (Cox *et al*, 2011) and an *Arabidopsis thaliana* reference database (Araport). Perseus
583 (Tyanova *et al*, 2016b) and Python 3.0 were used for statistical data analyses. For a targeted
584 analysis of the kinase assay data set, MS1 chromatograms from selected phosphopeptides were
585 extracted and analyzed using the Skyline software (MacLean *et al*, 2010). For detailed information
586 about LC-MS/MS data acquisition and analysis see supporting methods.
587
588 **Light and electron microscopy**
589 For scanning electron microscopy, a Zeiss (LEO) VP 438 microscope was operated at 15 kV.
590 Fresh seedlings were placed onto stubs and examined immediately in low vacuum. Confocal
591 microscopes used for imaging were an Olympus (www.olympus-ims.com) Fluoview 1000 confocal
592 laser scanning microscope (CSLM) and a Leica (www.leica-microsystems.com) SP8 Hyvolution
593 CSLM. 40x and 60x water immersion 0.9 numerical aperture objectives (Olympus) were used.
594 Imaging data were acquired using LAS-X software (Leica) and FV10-Ver.2.6.0 software
595 (Olympus). The following excitation and emission parameters were used for the respective
596 fluorescent proteins: YFP 514 nm excitation, 525-575 nm emission; GFP 488 nm excitation, 500-
597 550 nm emission; and FM4-64 emission at 640 nm. 10-day-old seedlings were stained with
598 modified pseudo-Schiff propidium iodide staining (Truernit *et al*, 2008). Excitation Laser was set
599 to 488 nm. The Emission was detected at 520 nm. The junction between the meristematic and
600 elongation zones was determined by marking the first cell in a single cortex cell file that was double
601 the length of the previous cell (González-García *et al*, 2011). For seedling images, a Leica S APO
602 stereo microscope with a Leica MC170 HD camera was used.
603
604 **Differential growth decision assay**
605 The differential growth decision experiment was performed as described by Kalbfuß *et al*, 2022.
606 In brief, seeds were surface sterilized using a brief 80% ethanol rinse followed by 15 min
607 incubation in sterilization buffer (0.01% SDS, 3% NaOCl). After 5 washes in mQ water, seeds
608 were resuspended in 0.15% agar and stratified in the dark at 4°C for 7 days to break seed
609 dormancy. Afterwards, seeds were plated on squared plates with exactly 45 ml ½ MS medium
610 supplemented with B5 Vitamins (Sigma). Culture media for TRS120 phosphomutants was
611 additionally supplemented with 50 µg/ml kanamycin to select for transgenic seedlings. For -0.4
612 MPa water deficit, media plates were infused with sterile-filtrated 45 ml 2x PEG-6000 (Merck
613 group; dissolved in liquid ½ MS media) for exactly 24 h at RT and afterwards the PEG-solution
614 completely decanted. Seeds were plated at the interface between the culture media and sterilized
615 plastic strips on the media such that, upon germination, only the root touched the agar. For water
616 stress, seeds in each biological replicate were sown on two plates for technical replicates which
617 were pooled for analysis. After plating plates were sealed with breathable tape. Plates for dark
618 conditions were wrapped with two layers of thick aluminum foil. All plates were incubated for 10
619 days at 22°C with permanent light (80 µmol $m^{-2}s^{-1}$). Note that the plates were negatively inclined
620 by 4° to promote root growth on the media surface rather than in the agar.
621 After incubation of 10 days seedlings were transferred onto cold 1.2% agar plates, scanned at
622 1200 ppi and saved as tiff files. Hypocotyl and root lengths were analyzed with Fiji - ImageJ using
623 the free-hand-tool. The ratio was calculated as hypocotyl length divided by root length.

624 Root and hypocotyl responses to water deficit in the dark (abbreviated as darkW) were
625 computed as

626 $$\frac{\text{organ length in the dark}}{\text{organ length under darkW}}$$

627

628 And for the ratio:

629 $$\text{ratio adjustment}=\frac{\left(\frac{\text{hypocotyl}}{\text{root}}\right)\text{dark}}{\left(\frac{\text{hypocotyl}}{\text{root}}\right)\text{darkW}}$$

630 Due to variability between PEG lots and PEG plates (Kalbfuß *et al*, 2022), we normalized each
631 mutant to the corresponding wild-type ecotype (see Table S1) on the same plate. Thus, the
632 normalized ratio adjustment to water stress in the dark (darkW) was computed as follows:

633 $$RQ_{ratio}=\frac{\text{ratio adjustment mutant}}{\text{ratio adjustment wild-type}}$$

634

635 $RQ_{hypocotyl}$ and RQ_{root} as well as light versus dark responses were computed in a similar fashion.
636 These normalized organ and ratio adjustments were referred to as response quotients (RQ) to
637 light-to-dark or dark-to-darkW conditions. The mean RQ_{ratio} of at least three biological replicates
638 (i.e. the seed stocks from different mother plants) is shown. Responses were considered to be
639 attenuated for $RQ_{ratio} < 0.8$, normal in the 0.8-1.2 range, and enhanced for $RQ_{ratio} > 1.2$. For volcano
640 plots we plotted the mean RQ_{ratio} on the X axis and the median P_{ratio}-value on the Y axis. Organ
641 and ratio adjustments for light-to-dark comparisons were computed as organ length (or ratio) in
642 the light divided by organ length (or ratio) in the dark. P-values were computed with the Student's
643 T-test. Responses were considered to be insignificant for P-values ≥ 0.05 and attenuated for P-
644 values ≥ 0.00001. The median P-value for at least three replicates is shown in the volcano plots.

645

646 **Germination assay under osmotic stress**

647 For germination curve experiments, surface-sterilized seeds were stratified in the dark at 4°C for
648 two days. Seeds were plated on ½ MS media supplemented with 0.05% B5 Vitamins (Sigma) and
649 either 0 mM, 200 mM, or 400 mM mannitol (Millipore). Approximately 100 seeds were plated per
650 condition. Plates were incubated at 22°C under constant light conditions (80 µmol $m^{-2}s^{-1}$) and
651 rotated every day. Seed germination rates were recorded every 24 h. Seeds were scored as
652 germinated when the radicle emerged. Data were obtained for three biological replicates, each
653 with three technical replicates.

654

655 **Western blot analysis**

656 Standard Western blot analysis was performed according to Sambrook *et al*, 1989. 7.5% SDS-
657 PAGE gels (Mini-PROTEAN TGX gels, Bio-Rad) were blotted onto PVDF Immobilon-FL
658 membranes (Millipore). Polyclonal rabbit anti-GFP antibody (1:2000; A11122, Invitrogen) was
659 used as primary antibody. As secondary antibody, we used a goat anti-rabbit Horseradish
660 peroxidase-conjugated antibody (1:6000; Pierce, Thermo Scientific) together with the SuperSignal
661 West Femto Maximum Sensitivity Substrate (Thermo Scientific). To check for equal loading, blots
662 were stained with Coomassie (10% acetic acid, 50% methanol, 0.25% Coomassie Blue R-250)
663 and subsequently destained (10% acetic acid, 50% methanol).

Statistical analysis and image processing

False discovery rates, determined with the standard two-tailed t-test, were set at a cut-off of 1. Images taken with the Leica SP8 microscope were deconvolved using the built-in Huygens Scientific deconvolution software (www.leica-microsystems.com) operated in 2D. For consistency in quantitative analyses, we selected cortical root tip cells, at a height of 6-22 cells above the quiescent center in the root apical meristem. Images were processed with Adobe photoshop (www.adobe.com) and GIMP (https://www.gimp.org) and analysed with Image J (https://imagej.nih.gov). Statistical analyses were performed in RStudio. Figures were created with RStudio's ggplot2 package and assembled with Inkscape (https://inkscape.org).

Acknowledgements

We thank Prof. Wilfried Schwab, Prof. Erwin Grill and other members of the botany department for their support. Thanks to Prof. Arne Skerra, Martin Schlapschy and Veder Garcia for useful suggestions. We thank Yannik Schreckenberg, Andreas Czempiel, Hermine Kienberger, Nina Lomp and Franziska Hackbarth for technical assistance. We thank the WZW/TUM Centre for Advanced Light Microscopy (CALM), headed by Ramon Torres-Ruiz and Klaus Michel, for access to confocal microscopes, and Prof. Kay Schneitz for access to their Leica S APO stereo microscope. Thanks to Roman Meier at the TUMmesa facility, directed by Leonardo Teixeira, for supporting us with optimal growth conditions for our plants. Jorge José Casal and Sean Cutler shared published resources.

Data deposition

Mass spectrometry data have been deposited with the ProteomeXchange Consortium via the PRoteomics IDEntification (PRIDE) partner repository (Perez-Riverol *et al*, 2019) or the Mass Spectrometry Interactive Virtual Environment data repository (MassIVE; http://massive.ucsd.edu). The CLUB-GFP IP-MS data has previously been deposited (Kalde *et al*, 2019) and can be accessed with the dataset identifier PXD013016. All other IP-MS or MS datasets are being deposited here for the first time. The proteomics raw data, MaxQuant search results and used protein sequence databases for the other datasets can be accessed using the MassIVE data set identifier [pending]. All targeted proteomic raw data and Skyline analysis files have been deposited to Panorama Public (Sharma *et al*, 2014, 2018) [pending].

Funding

This work was supported by Deutsche Forschungsgemeinschaft DFG grants AS110/5-2, AS110/8-1 & AS110/10-1 as well as BaCaTEC Nr. 14 [2018-2] to F.F.A., by the European Research Council's Horizon 2020 Research and Innovation Programme (Grant Agreement 648420) grant to P.F-B., and by National Institutes of Health (R01GM066258 to Z.-Y.W.). M. Abele and C.L. were supported by the EU Horizon 2020 grant Epic-XS. TUMmesa was funded with support of the German Science Foundation (DFG, INST 95/1184-1 FUGG).

Conflict of interest

The authors declare no conflict of interest.

Author contributions

Conceptualization: FFA
Methodology: MA, CL, BA, CHP, PFB, CW, AS, NK, ASM, BB, CM, EF, FFA
Investigation: CW, MA, BA, MAM, AS, NK, ASM, RR, CHP, BB, CM, EF, FFA
Visualization: CW, MA, BA, MAM, AS, NK, ASM, RR, CHP, BB, CM
Funding acquisition: DWE, PFB, ZW, CL, FFA
Project administration: FFA
Supervision: EF, DWE, PFB, ZW, CL, FFA
Writing - original draft: FFA
Writing - review & editing: CW, MA, BA, NK, ASM, RR, CHP, BB, CM, PFB, ZW, CL, FFA

REFERENCES

Altmann M, Altmann S, Falter C & Falter-Braun P (2018) High-Quality Yeast-2-Hybrid Interaction Network Mapping. *Curr Protoc Plant Biol* 3: e20067

Asaoka R, Uemura T, Ito J, Fujimoto M, Ito E, Ueda T & Nakano A (2013) Arabidopsis RABA1 GTPases are involved in transport between the trans-Golgi network and the plasma membrane, and are required for salinity stress tolerance. *Plant J* 73: 240–249

Assaad FF, Huet Y, Mayer U & Jürgens G (2001) The Cytokinesis Gene KEULE Encodes a Sec1 Protein That Binds the Syntaxin KNOLLE. *J Cell Biol* 152: 531–543

Boutté Y, Jonsson K, McFarlane HE, Johnson E, Gendre D, Swarup R, Friml J, Samuels L, Robert S & Bhalerao RP (2013) ECHIDNA-mediated post-Golgi trafficking of auxin carriers for differential cell elongation. *Proc Natl Acad Sci U S A* 110: 16259–16264

Cai Y, Chin HF, Lazarova D, Menon S, Fu C, Cai H, Sclafani A, Rodgers DW, De La Cruz EM, Ferro-Novick S, *et al* (2008) The Structural Basis for Activation of the Rab Ypt1p by the TRAPP Membrane-Tethering Complexes. *Cell* 133: 1202–1213

Clark NM, Nolan TM, Wang P, Song G, Montes C, Valentine CT, Guo H, Sozzani R, Yin Y & Walley JW (2021) Integrated omics networks reveal the temporal signaling events of brassinosteroid response in Arabidopsis. *Nat Commun* 12: 5858

Cox J & Mann M (2008) MaxQuant enables high peptide identification rates, individualized p.p.b.-range mass accuracies and proteome-wide protein quantification. *Nat Biotechnol* 26: 1367–1372

Cox J, Neuhauser N, Michalski A, Scheltema RA, Olsen J V. & Mann M (2011) Andromeda: A Peptide Search Engine Integrated into the MaxQuant Environment. *J Proteome Res* 10: 1794–1805

Dai L, Wang B, Wang T, Meyer EH, Kettel V, Hoffmann N, McFarlane HE, Li S, Wu X, Picard KL, *et al* (2022) The TOR complex controls ATP levels to regulate actin cytoskeleton dynamics in Arabidopsis. *Proc Natl Acad Sci U S A* 119: e2122969119

Darwin C (2009) The Power of Movement in Plants Cambridge University Press

Ding Z, Galván-Ampudia CS, Demarsy E, Łangowski Ł, Kleine-Vehn J, Fan Y, Morita MT, Tasaka M, Fankhauser C, Offringa R, *et al* (2011) Light-mediated polarization of the PIN3 auxin transporter for the phototropic response in Arabidopsis. *Nat Cell Biol* 13: 447–452

Dong L, Wang Z, Liu J & Wang X (2020) AtSK11 and AtSK12 Mediate the Mild Osmotic Stress-Induced Root Growth Response in Arabidopsis. *Int J Mol Sci* 21: 1–16

Elliott L, Moore I & Kirchhelle C (2020) Spatio-temporal control of post-Golgi exocytic trafficking in plants. *J Cell Sci* 133: jcs237065

Ericsson T (1995) Growth and shoot: root ratio of seedlings in relation to nutrient availability. *Plant Soil* 168: 205–214

Fan X, Yang C, Klisch D, Ferguson A, Bhaellero RP, Niu X & Wilson ZA (2014) ECHIDNA Protein Impacts on Male Fertility in Arabidopsis by Mediating trans-Golgi Network Secretory Trafficking during Anther and Pollen Development. *Plant Physiol* 164: 1338–1349

Friml J, Wiśniewska J, Benková E, Mendgen K & Palme K (2002) Lateral relocation of auxin efflux regulator PIN3 mediates tropism in Arabidopsis. *Nature* 415: 806–809

Galviz YCF, Ribeiro R V. & Souza GM (2020) Yes, plants do have memory. *Theor Exp Plant Physiol* 32: 195–202

Garcia VJ, Xu S-L, Ravikumar R, Wang W, Elliott L, Gonzalez E, Fesenko M, Altmann M, Brunschweiger B, Falter-Braun P, *et al* (2020) TRIPP Is a Plant-Specific Component of the Arabidopsis TRAPPII Membrane Trafficking Complex with Important Roles in Plant Development. *Plant Cell* 32: 2424–2443

Garzón PC & Keijzer F (2011) Plants: Adaptive behavior, root-brains, and minimal cognition. *Adapt Behav* 19: 155–171

Gendre D, Jonsson K, Boutté Y & Bhalerao RP (2015) Journey to the cell surface—the central

773 role of the trans-Golgi network in plants. *Protoplasma* 252: 385–398
774 Gendre D, McFarlane HE, Johnson E, Mouille G, Sjödin A, Oh J, Levesque-Tremblay G,
775 Watanabe Y, Samuels L & Bhalerao RP (2013) Trans-Golgi Network Localized
776 ECHIDNA/Ypt Interacting Protein Complex Is Required for the Secretion of Cell Wall
777 Polysaccharides in Arabidopsis. *Plant Cell* 25: 2633–2646
778 Gendre D, Oh J, Boutté Y, Best JG, Samuels L, Nilsson R, Uemura T, Marchant A, Bennett MJ,
779 Grebe M, *et al* (2011) Conserved Arabidopsis ECHIDNA protein mediates trans-Golgi-
780 network trafficking and cell elongation. *Proc Natl Acad Sci U S A* 108: 8048–8053
781 González-García M-P, Vilarrasa-Blasi J, Zhiponova M, Divol F, Mora-García S, Russinova E &
782 Caño-Delgado AI (2011) Brassinosteroids control meristem size by promoting cell cycle
783 progression in Arabidopsis roots. *Development* 138: 849–859
784 Jaber E, Thiele K, Kindzierski V, Loderer C, Rybak K, Jürgens G, Mayer U, Söllner R, Wanner G
785 & Assaad FF (2010) A putative TRAPPII tethering factor is required for cell plate assembly
786 during cytokinesis in Arabidopsis. *New Phytol* 187: 751–763
787 Jiménez JL, Hegemann B, Hutchins JRA, Peters J-M & Durbin R (2007) A systematic
788 comparative and structural analysis of protein phosphorylation sites based on the mtcPTM
789 database. *Genome Biol* 8: R90
790 Jumper J, Evans R, Pritzel A, Green T, Figurnov M, Ronneberger O, Tunyasuvunakool K, Bates
791 R, Žídek A, Potapenko A, *et al* (2021) Highly accurate protein structure prediction with
792 AlphaFold. *Nature* 596: 583–589
793 Kalbfuß N, Strohmayr A, Kegel M, Le L, Grosse-Holz F, Brunschweiger B, Stöckl K, Wiese C,
794 Franke C, Schiestl C, *et al* (2022) A role for brassinosteroid signalling in decision-making
795 processes in the Arabidopsis seedling. *PLoS Genet* 18: e1010541
796 Kalde M, Elliott L, Ravikumar R, Rybak K, Altmann M, Klaeger S, Wiese C, Abele M, Al B,
797 Kalbfuß N, *et al* (2019) Interactions between Transport Protein Particle (TRAPP) complexes
798 and Rab GTPases in Arabidopsis. *Plant J* 100: 279–297
799 Karban R & Orrock JL (2018) A judgment and decision-making model for plant behavior.
800 *Ecology* 99: 1909–1919
801 Kim S-J & Bassham DC (2011) TNO1 Is Involved in Salt Tolerance and Vacuolar Trafficking in
802 Arabidopsis. *Plant Physiol* 156: 514–526
803 Kim T-W, Michniewicz M, Bergmann DC & Wang Z-Y (2012) Brassinosteroid regulates stomatal
804 development by GSK3-mediated inhibition of a MAPK pathway. *Nature* 482: 419–422
805 Kim T-W, Park CH, Hsu C-C, Kim Y-W, Ko Y-W, Zhang Z, Zhu J-Y, Hsiao Y-C, Branon T,
806 Kaasik K, *et al* (2023) Mapping the signaling network of BIN2 kinase using TurboID-
807 mediated biotin labeling and phosphoproteomics. *Plant Cell* 35: 975–993
808 Lee C-F, Pu H-Y, Wang L-C, Sayler RJ, Yeh C-H & Wu S-J (2006) Mutation in a homolog of
809 yeast Vps53p accounts for the heat and osmotic hypersensitive phenotypes in Arabidopsis
810 hit1-1 mutant. *Planta* 224: 330–338
811 Li C, Zhang B & Yu H (2021) GSK3s: nodes of multilayer regulation of plant development and
812 stress responses. *Trends Plant Sci* 26: 1286–1300
813 Li J & Nam KH (2002) Regulation of Brassinosteroid Signaling by a GSK3/SHAGGY-Like
814 Kinase. *Science* 295: 1299–1301
815 Liu L, Qin L, Safdar L Bin, Zhao C, Cheng X, Xie M, Zhang Y, Gao F, Bai Z, Huang J, *et al*
816 (2023) The plant trans-Golgi network component ECHIDNA regulates defense, cell death,
817 and endoplasmic reticulum stress. *Plant Physiol* 191: 558–574
818 Lv M & Li J (2020) Molecular Mechanisms of Brassinosteroid-Mediated Responses to Changing
819 Environments in Arabidopsis. *Int J Mol Sci* 21: 2737
820 MacLean B, Tomazela DM, Shulman N, Chambers M, Finney GL, Frewen B, Kern R, Tabb DL,
821 Liebler DC & MacCoss MJ (2010) Skyline: an open source document editor for creating and
822 analyzing targeted proteomics experiments. *Bioinformatics* 26: 966–968
823 McClung CR (2006) Plant Circadian Rhythms. *Plant Cell* 18: 792–803

McFarlane HE, Watanabe Y, Gendre D, Carruthers K, Levesque-Tremblay G, Haughn GW, Bhalerao RP & Samuels L (2013) Cell Wall Polysaccharides are Mislocalized to the Vacuole in echidna Mutants. *Plant Cell Physiol* 54: 1867–1880

Naramoto S, Nodzyński T, Dainobu T, Takatsuka H, Okada T, Friml J & Fukuda H (2014) VAN4 Encodes a Putative TRS120 That is Required for Normal Cell Growth and Vein Development in Arabidopsis. *Plant Cell Physiol* 55: 750–763

Perez-Riverol Y, Csordas A, Bai J, Bernal-Llinares M, Hewapathirana S, Kundu DJ, Inuganti A, Griss J, Mayer G, Eisenacher M, *et al* (2019) The PRIDE database and related tools and resources in 2019: improving support for quantification data. *Nucleic Acids Res* 47: D442–D450

Pinar M, Arias-Palomo E, de los Ríos V, Arst HNJ & Peñalva MA (2019) Characterization of Aspergillus nidulans TRAPPs uncovers unprecedented similarities between fungi and metazoans and reveals the modular assembly of TRAPPII. *PLoS Genet* 15: e1008557

Planas-Riverola A, Gupta A, Betegón-Putze I, Bosch N, Ibañes M & Caño-Delgado AI (2019) Brassinosteroid signaling in plant development and adaptation to stress. *Development* 146: dev151894

Polko JK, van Zanten M, van Rooij JA, Marée AFM, Voesenek LACJ, Peeters AJM & Pierik R (2012) Ethylene-induced differential petiole growth in Arabidopsis thaliana involves local microtubule reorientation and cell expansion. *New Phytol* 193: 339–348

Qi X, Kaneda M, Chen J, Geitmann A & Zheng H (2011) A specific role for Arabidopsis TRAPPII in post-Golgi trafficking that is crucial for cytokinesis and cell polarity. *Plant J* 68: 234–248

Rauf M, Arif M, Fisahn J, Xue G-P, Balazadeh S & Mueller-Roeber B (2013) NAC Transcription Factor SPEEDY HYPONASTIC GROWTH Regulates Flooding-Induced Leaf Movement in Arabidopsis. *Plant Cell* 25: 4941–4955

Ravikumar R, Kalbfuß N, Gendre D, Steiner A, Altmann M, Altmann S, Rybak K, Edelmann H, Stephan F, Lampe M, *et al* (2018) Independent yet overlapping pathways ensure the robustness and responsiveness of trans-Golgi network functions in Arabidopsis. *Development* 145: dev169201

Ravikumar R, Steiner A & Assaad FF (2017) Multisubunit tethering complexes in higher plants. *Curr Opin Plant Biol* 40: 97–105

Rosquete MR & Drakakaki G (2018) Plant TGN in the stress response: a compartmentalized overview. *Curr Opin Plant Biol* 46: 122–129

Rosquete MR, Worden N, Ren G, Sinclair RM, Pfleger S, Salemi M, Phinney BS, Domozych D, Wilkop T & Drakakaki G (2019) AtTRAPPC11/ROG2: A Role for TRAPPs in Maintenance of the Plant Trans-Golgi Network/Early Endosome Organization and Function. *Plant Cell* 31: 1879–1898

Rybak K, Steiner A, Synek L, Klaeger S, Kulich I, Facher E, Wanner G, Kuster B, Zarsky V, Persson S, *et al* (2014) Plant Cytokinesis Is Orchestrated by the Sequential Action of the TRAPPII and Exocyst Tethering Complexes. *Dev Cell* 29: 607–620

Sambrook J, Fritsch EF & Maniatis T (1989) Molecular Cloning: A Laboratory Manual Cold Spring Harbor Laboratory Press

Seki M, Carninci P, Nishiyama Y, Hayashizaki Y & Shinozaki K (1998) High-efficiency cloning of Arabidopsis full-length cDNA by biotinylated CAP trapper. *Plant J* 15: 707–720

Seki M, Narusaka M, Kamiya A, Ishida J, Satou M, Sakurai T, Nakajima M, Enju A, Akiyama K, Oono Y, *et al* (2002) Functional Annotation of a Full-Length Arabidopsis cDNA Collection. *Science* 296: 141–145

Severino LS (2021) Plants make smart decisions in complex environments. *Plant Signal Behav* 16: 1970448

Sharma V, Eckels J, Schilling B, Ludwig C, Jaffe JD, MacCoss MJ & MacLean B (2018) Panorama Public: A Public Repository for Quantitative Data Sets Processed in Skyline. *Mol Cell Proteomics* 17: 1239–1244

875 Sharma V, Eckels J, Taylor GK, Shulman NJ, Stergachis AB, Joyner SA, Yan P, Whiteaker JR,
876 Halusa GN, Schilling B, *et al* (2014) Panorama: A Targeted Proteomics Knowledge Base. *J*
877 *Proteome Res* 13: 4205–4210
878 Shevchenko A, Tomas H, Havli J, Olsen J V & Mann M (2006) In-gel digestion for mass
879 spectrometric characterization of proteins and proteomes. *Nat Protoc* 1: 2856–2860
880 Silvertown J & Gordon DM (1989) A Framework for Plant Behavior. *Annu Rev Ecol Syst* 20:
881 349–366
882 Söllner R, Glässer G, Wanner G, Somerville CR, Jürgens G & Assaad FF (2002) Cytokinesis-
883 Defective Mutants of Arabidopsis. *Plant Physiol* 129: 678–690
884 Song Y, Wang Y, Yu Q, Sun Y, Zhang J, Zhan J & Ren M (2023) Regulatory network of GSK3-
885 like kinases and their role in plant stress response. *Front Plant Sci* 14: 1123436
886 Steiner A, Rybak K, Altmann M, McFarlane HE, Klaeger S, Nguyen N, Facher E, Ivakov A,
887 Wanner G, Kuster B, *et al* (2016) Cell cycle-regulated PLEIADE/AtMAP65-3 links
888 membrane and microtubule dynamics during plant cytokinesis. *Plant J* 88: 531–541
889 Swarbreck D, Wilks C, Lamesch P, Berardini TZ, Garcia-Hernandez M, Foerster H, Li D, Meyer
890 T, Muller R, Ploetz L, *et al* (2008) The Arabidopsis Information Resource (TAIR): gene
891 structure and function annotation. *Nucleic Acids Res* 36: D1009–D1014
892 Thellmann M, Rybak K, Thiele K, Wanner G & Assaad FF (2010) Tethering Factors Required for
893 Cytokinesis in Arabidopsis. *Plant Physiol* 154: 720–732
894 Thomas LL, van der Vegt SA & Fromme JC (2019) A Steric Gating Mechanism Dictates the
895 Substrate Specificity of a Rab-GEF. *Dev Cell* 48: 100–114
896 Truernit E, Bauby H, Dubreucq B, Grandjean O, Runions J, Barthélémy J & Palauqui J-C (2008)
897 High-Resolution Whole-Mount Imaging of Three-Dimensional Tissue Organization and
898 Gene Expression Enables the Study of Phloem Development and Structure in Arabidopsis.
899 *Plant Cell* 20: 1494–1503
900 Tyanova S, Temu T & Cox J (2016a) The MaxQuant computational platform for mass
901 spectrometry-based shotgun proteomics. *Nat Protoc* 11: 2301–2319
902 Tyanova S, Temu T, Sinitcyn P, Carlson A, Hein MY, Geiger T, Mann M & Cox J (2016b) The
903 Perseus computational platform for comprehensive analysis of (prote)omics data. *Nat*
904 *Methods* 13: 731–740
905 Uemura T (2016) Physiological Roles of Plant Post-Golgi Transport Pathways in Membrane
906 Trafficking. *Plant Cell Physiol* 57: 2013–2019
907 Uemura T, Ueda T & Nakano A (2012) The physiological role of SYP4 in the salinity and osmotic
908 stress tolerances. *Plant Signal Behav* 7: 1118–1120
909 Varadi M, Anyango S, Deshpande M, Nair S, Natassia C, Yordanova G, Yuan D, Stroe O, Wood
910 G, Laydon A, *et al* (2022) AlphaFold Protein Structure Database: massively expanding the
911 structural coverage of protein-sequence space with high-accuracy models. *Nucleic Acids*
912 *Res* 50: D439–D444
913 Wang L-C, Tsai M-C, Chang K-Y, Fan Y-S, Yeh C-H & Wu S-J (2011) Involvement of the
914 Arabidopsis HIT1/AtVPS53 tethering protein homologue in the acclimation of the plasma
915 membrane to heat stress. *J Exp Bot* 62: 3609–3620
916 Whippo CW & Hangarter RP (2009) The 'sensational' power of movement in plants: A Darwinian
917 system for studying the evolution of behavior. *Am J Bot* 96: 2115–2127
918 Yin C, Karim S, Zhang H & Aronsson H (2017) Arabidopsis RabF1 (ARA6) Is Involved in Salt
919 Stress and Dark-Induced Senescence (DIS). *Int J Mol Sci* 18: 309
920 Youn J-H & Kim T-W (2015) Functional Insights of Plant GSK3-like Kinases: Multi-Taskers in
921 Diverse Cellular Signal Transduction Pathways. *Mol Plant* 8: 552–565
922 Zhao R, Li N, Lin Q, Li M, Shen X, Peng Y, Du Y, Ning Q, Li Y, Zhan J, *et al* (2023) ZmBET5L1
923 inhibits primary root growth and decreases osmotic stress tolerance by mediating vesicle
924 aggregation and tethering in maize. *Plant Cell Environ* 46: 975–990
925 Zhu J, Gong Z, Zhang C, Song C-P, Damsz B, Inan G, Koiwa H, Zhu J-K, Hasegawa PM &

926 Bressan RA (2002) OSM1/SYP61: A Syntaxin Protein in Arabidopsis Controls Abscisic
927 Acid-Mediated and Non-Abscisic Acid-Mediated Responses to Abiotic Stress. *Plant Cell* 14:
928 3009–3028
929

930 **FIGURE LEGENDS**

931

932 **Figure 1. The TRAPPII interactome.**

933 **A.** Gene ontology (GO) term enrichment analysis of the TRAPPII interactome. Depicted are fold
934 enrichments of GO terms of level 0 as bar plots colored by significance level. The data are derived
935 from an analysis of IP-MS from inflorescences with the TRAPPII-specific subunit CLUB-GFP as
936 bait (see Fig. 1B; Kalde *et al*, 2019). Terms are grouped by manually annotated super-categories.
937 Metabolic processes were excluded for simplification. Note that the super categories organization
938 (9) and traffic/transport (12) make up the majority of GO terms (21/49) and that response to
939 stimulus (11) comprises the second largest category. Cutoffs were set at 1.5 for fold-change and
940 0.003 for the *P*-value, which was adjusted for the false discovery rate.

941 **B.** IP-MS with the TRAPPII-specific subunit CLUB-GFP as bait (Kalde *et al*, 2019). Inflorescences
942 were used. Each protein was present in all three biological replicates. The ratio (or fold-change)
943 was calculated for each protein as the average intensity of the signal in the experiment divided by
944 its average intensity in the soluble GFP empty vector control. The *P*-value (depicted along a
945 negative log10 scale) is plotted against the signal ratio. Dotted grey lines represent cutoffs: *P*-
946 value < 0.02 and Ratio > 8 or > 5. Note that TRAPPII subunits (light blue for core TRAPP; dark
947 blue for TRAPPII-specific subunits; the AtTRS130/CLUB-GFP TRAPPII-specific bait is depicted
948 as an open circle) are in the upper right field, indicating high abundance and good reproducibility.
949 AtSKs (magenta), MAP65-1 (orange) and Rab A2a GTPase (green) are all in the upper middle
950 field; these may be transient interactors of TRAPPII. Note that AtSKs (AtSK11/12/32) are more
951 significant than validated interactors such as MAP65 and RabA2a (Kalde *et al*, 2019; Steiner *et*
952 *al*, 2016).

953 **C.** Yeast two-hybrid assays of interactions between BIN2 and TRAPPII subunits. BIN2 was fused
954 to the GAL4 DNA-binding domain (DB) and TRAPPII subunits and truncations thereof (CLUB$^{1\text{-}417}$,
955 CLUB$^{392\text{-}1260}$, CLUB$^{792\text{-}1260}$, TRS120$^{1\text{-}800}$, TRS120$^{499\text{-}1187}$ and TRS120$^{750\text{-}1187}$; referred to below as
956 CLUB-C1, -C2, -C3 and TRS120-T1, -T2, -T3) to the GAL4 activation domain (AD). As negative
957 control, the BIN2-DB construct was tested with the empty AD vector. Interactions were verified by
958 pairwise one-on-one mating in four independent replicate experiments. The panels are from
959 different plates. The results show interactions between BIN2 and AtTRS120$^{499\text{-}1187}$ wild-type. BIN2
960 bound specifically to the TRAPPII subunit TRS120 (TRS120$^{499\text{-}1187}$ / T2 truncation) and not with
961 other TRAPPII subunits or truncations. In a total of > 2400 pairwise tests, BIN2 was the only kinase
962 we found that interacted with a TRAPP subunit. The Y2H did not detect AtTRS130/CLUB-BIN2
963 interaction shown in Fig. 1B, which shows co-purified proteins that can include indirect - as

964 opposed to binary - interactors. Related to Fig. S1.
965
966
967 **Figure 2. GSK3/AtSK sites in TRAPPII and binary interactions.**
968 **A.** TRAPPII-specific truncations for yeast two-hybrid were based on phylogenetic analysis (Steiner
969 *et al*, 2016). Conserved sequences are depicted in red, intermediate degrees of conservation in
970 orange, and plant-specific sequences are in green. All three GSK3 sites found to be
971 phosphorylated *in vivo* (delineated by a blue rectangle) reside in the plant-specific moiety of
972 TRS120-T2 (green).
973 **B.** GSK3 sites in TRS120-T2. The α-phosphosite of AtTRS120 spans amino acid positions S922
974 and S923, the β-phosphosite amino acids S971-S975 and the γ-phosphosite amino acid residue
975 S1165. The canonical GSK3 consensus sequence is: (pS/pT)*XXX*(S/T), and the β-phosphosite
976 fits this definition (see underlined SXXXS). Even though they are annotated as GSK3 sites in the
977 PPSP (https://www.phosphosite.org) database, the α-phosphosite deviates somewhat with
978 SXXXXS, and the γ-phosphosite deviates completely. Amino acids in red were mutated to A or D
979 via site-directed mutagenesis. Amino acids highlighted in yellow were found to be phosphorylated
980 *in vivo* and these were all serines (see Fig. S2).
981 **C, D.** Mapping of GSK3/AtSK sites on an Alphafold structural prediction (Jumper *et al*, 2021;
982 Varadi *et al*, 2022) of AtTRS120. A lateral view (C) and a frontal perspective (D) are shown. Note
983 that all three GSK3/AtSK sites reside in unstructured, flexible and accessible regions of the
984 protein.
985 **E.** The Arabidopsis TRAPPII complex consists of six shared core subunits (light blue) and three
986 TRAPPII-specific subunits (CLUB/AtTRS130, AtTRS120 and the plant-specific subunit TRIPP),
987 and forms a dimer with plant-specific domains (green) at the predicted dimer interface (Garcia *et*
988 *al*, 2020; Kalde *et al*, 2019). A Rab-GTPase (beige) is shown to bind core-TRAPP subunits at the
989 approximate location of the putative GEF catalytic site, based on yeast models (Cai *et al*, 2008;
990 Thomas *et al*, 2019).
991 **F.** Yeast two-hybrid assays of interactions between BIN2 and TRAPPII truncations (CLUB-C2,
992 CLUB-C3, TRS120-T1, TRS120-T3), as positive controls, fused to the GAL4 DNA-binding domain
993 (DB) and TRS120-T2 truncation and its phosphomutants TRS120-T2 SαD, SβD, SγD, SαβD and
994 SαβγD fused to the GAL4 activation domain (AD). As negative control, the BIN2-DB construct was
995 tested with the empty AD vector. Interactions were verified by pairwise one-on-one mating in four
996 independent replicate experiments; for the control (Co) only one representative example is shown.
997 The panels are from different plates. The results show interactions between BIN2 and AtTRS120-

998 T2 wild-type and phosphovariants; there was, however, no reproducible interaction if all three
999 target sites were phosphomimetic. Related to Fig. S1-S5.
1000
1001
1002 **Figure 3. *In vitro* AtSK kinase assays with TRS120 as bait.**
1003 **A.** *In vitro* kinase assays using GST:AtSK11 (72 kDa) and GST:TRS120-T2 (100 kDa). The
1004 change of phosphosignal is shown in a representative autoradiograph (upper panel) and the
1005 loaded protein amount in the corresponding CBB (lower panel). Non-phosphorylated variants were
1006 used as negative controls. The means ±SD of phosphosignals were normalized to the protein
1007 amount; nonmutated TRS120-T2 WT is set at 1.0 (right panel); n = 3 independent experiments; *:
1008 P<0.05 paired two-sided student's t-test; TRS120-T2-SαβγA versus TRS120-T2 WT).
1009 **B.** AtTRS120-T2 has highly (red) and moderately (orange) conserved sequences, as well as plant-
1010 specific sequences (green). Three GSK3 sites (referred to as α, β, γ; see Fig. 2B) can be found in
1011 the plant-specific T2 domain.
1012 **C.** Kinase assays were performed *in vitro* with mass-spectrometry readout. One member of each
1013 shaggy-like kinase clade (AtSKs; see Fig. S3A) was used with the TRS120-T2 truncation as
1014 substrate. Dilution series are depicted in different shades of blue. AtSKs in clades I-III differentially
1015 phosphorylate the substrate at three GSK3 consensus sites (with a preference for the γ site) in a
1016 time-dependent and concentration-dependent manner. A clade IV AtSK did not phosphorylate at
1017 all. Samples incubated for 120 min in a kinase buffer without ATP, or samples in which the kinase
1018 was heat inactivated, served as negative controls. The numbers in grey in each plot denote the
1019 number of times the phosphorylation event was seen in the given number of independent
1020 replicates. Note the higher intensity of the TRS120-γ peptide, especially for Clade I/SK11 (1e8 for
1021 TRS120-γ versus 1e6 for TRS120-α and TRS120-β on the Y axis). Related to Fig. S1-S6.
1022
1023
1024 **Figure 4. Role of the TRAPPII complex versus ECHIDNA in hypocotyl/root tradeoffs.**
1025 Seedlings were germinated on ½ MS in the dark (dark) or in dark with -0.4MPa water stress
1026 (darkW). **A.** Col-0 (wild-type). **B.** BR signaling mutant *bin2-3bil1bil2* triple knockout (from Kalbfuß
1027 *et al*, 2022). **C.** *club-2*, a null *trappii* mutant. **D.** *trs120-4*, a null *trappii* allele. **E.** *echidna* null allele,
1028 impaired in TGN structure and function. At least 3 experiments were performed for each line, and
1029 a representative one is shown here on the basis of RQ and *P*-values. **F.** Violin plot for a direct
1030 comparison between *trs120-4* and the corresponding wild-type (Col-0; in the same experiment
1031 and on the same PEG plates) showing that the response to a shift from dark to darkW seen in the

1032 wild-type was not observed in *trs120-4*. **G.** Normalized response quotient RQ_{ratio}. Each replicate
1033 is represented by a dot. Note that the triple *bin2-3bil1bil2* knock out, *trs120-4* and *club-2* had
1034 attenuated responses (magenta arrows). **H.** Volcano plot with the mean RQ_{ratio} depicted on the X
1035 axis and the median *P*-value of the response on the Y axis (negative log scale; a median of all
1036 replicates was used). The area shaded in grey on the red line (green arrow) is where wild-type
1037 ecotypes would theoretically map onto the plot. Mutants in the lower left quadrant (peach shading)
1038 were considered to have a "confused decision phenotype" (see text). *trs120-4* mutants mapped to
1039 the lower left quadrant and qualified as decision mutants on two counts: (i) a consistently opposite
1040 hypocotyl response (red asterisk in D), (ii) failure to adjust the hypocotyl/root ratio to darkW (the
1041 ratio for darkW is the same as for dark in panel D), translating into a non-significant *P*-value for
1042 the ratio response (H). The number (n) of seedlings measured per condition is in grey below the
1043 mean ±SD bar graphs. *P*-values were computed with a two-tailed student's t-test and are
1044 represented as follows: *: P<0.05; **: P<0.01; ***: P<0.001; ****: P<0.0001; *****: P<0.00001.
1045 Mutant alleles and the corresponding ecotypes are described in Table S1. See related Fig. S7.
1046
1047
1048 **Figure 5. Cell elongation in *trappii* hypocotyls under additive stress.**
1049 **A.** Col-0 wild-type.
1050 **B.** *club-2,* null *trappii* allele.
1051 **C.** *trs120-4,* null *trappii* allele.
1052 Seedlings were germinated in the light, or in the dark with (darkW) or without (dark) water stress
1053 (PEG -0.4MPa). The cellular growth parameters width and height were measured based on SEM
1054 images. The cell surface area was calculated as the product of cell width and length. The *trappii*
1055 mutants, *club-2* and *trs120-4*, showed the opposite hypocotyl cell height and cell surface
1056 adaptations to dark-to-darkW conditions (red asterisks in B and C) than the wild-type control.
1057 Representative SEM images of seedlings grown under the specified conditions are shown
1058 (scalebar = 20 µm). The sample size (n) is given as the number of cells/ number of seedlings that
1059 were analyzed in grey below the graph. Shown are means ±SD. *P*-values were computed with a
1060 two-tailed student's t-test and are represented as follows: ***: P<0.001; ****: P<0.0001; *****:
1061 P<0.00001.
1062
1063

1064 **Figure 6. Root meristem properties of *trappii* mutants under single versus additive stress**
1065 **conditions.** Seedlings were grown in the light (orange), dark (black) or dark with -0.4MPa water
1066 stress (darkW; blue).
1067 **A-D.** Col-0 wild-type.
1068 **E-H.** *trs120-4* null mutant.
1069 (A-C) and (E-G) confocal micrographs of mPS-PI stained root tips under different environmental
1070 conditions; black arrows mark the junction between the meristematic and elongation zones.
1071 **D, H.** 10 days after incubation, the cell lengths were measured in single cortex cell files, starting
1072 at the cortex/endodermis initials. The fitted lines were generated with Local Polynomial Regression
1073 Fitting with the 'loess' method in R; grey shading designates the 95 percent confidence interval.
1074 Cell lengths of consecutive cells as a function of cell number from the quiescent centre (QC); the
1075 green arrows point to the steep slope under the dark condition and steeper slope under darkW
1076 condition - the initiation of elongation - in the wild-type (D); magenta arrows point to flatter,
1077 unadjusted slopes under dark versus darkW in *trappii* (*trs120-4*) mutants (H). The sample size (n)
1078 is given as the number of cells/ number of seedlings that were analyzed in panels (D,H). Scale
1079 bar is 50 µm.
1080
1081
1082 **Figure 7. Responses of TRS120 phosphovariants to osmotic or additive stress.**
1083 Phosphovariants of P_{TRS120}::TRS120-GFP (Rybak *et al*, 2014) were in *trs120-4* homozygous
1084 backgrounds with the exception of the TRS120-SαβγD variant in panels A-C, which was in a
1085 hemizygous *trs120-4*/+ background.
1086 **A-C.** Germination of TRS120 phosphovariants under osmotic stress**.** Effect of A) 0 mM, B) 200
1087 mM and C) 400 mM mannitol on seed germination of the TRS120-SαβγA, the TRS120-SαβγD
1088 mutants and the following controls: Col-0 wild-type; the ABA deficient mutant *aba2-1* and the ABA
1089 PP2C co receptor triple knock-out line *hab1-1 abi1-2 pp2ca-1*. The non-phosphorylatable
1090 TRS120-SαβγA mutation increased seed germination on higher mannitol concentrations, whereas
1091 the phosphomimetic TRS120-SαβγD decreased seed germination. Shown are the means ± SD of
1092 three technical replicates. Similar results were obtained in three independent biological replicates.
1093 Stars indicate statistical significance compared to the wild-type Col-0 calculated with a two-tailed
1094 student's t-test (*: P<0.05; **: P<0.01; ***: P<0.001; ****: P<0.0001; *****: P<0.00001). DAS: days
1095 after stratification.
1096 **D-F**. Response quotients (RQ) of A) the hypocotyl, B) the root and C) the hypocotyl/root ratio of
1097 the non-phosphorylatable TRS120-SαβγA and the phosphomimetic TRS120-SαβγD mutants for

1098 dark-to-dark with water stress (-0.4MPa, darkW) adaptation. The divergent hypocotyl and root
1099 responses of TRS120-SαβγA and TRS120-SαβγD mutants resulted in a strong hypocotyl/root
1100 ratio phenotype under darkW conditions compared to the TRS120-WT control. TRS120-SαβγA
1101 showed an enhanced ratio adaption, whereas TRS120-SαβγD mutants had an attenuated ratio
1102 response. RQ response quotients are normalized to the rescue mutant TRS120-WT
1103 (P_{TRS120}::TRS120-GFP in *trs120-4/trs120-4*). A value of 1 (vertical red line) corresponds to an
1104 identical adaptation to darkW conditions as the rescue mutant. Dots represent biological
1105 replicates, of which there were a total of four primary transformants per line. Mean RQ values are
1106 given on the right.
1107
1108
1109 **Figure 8. Flow diagram suggesting how BIN2 might mediate plant adaptive responses by**
1110 **phosphorylating the TRAPPII complex.**
1111 Shaggy-like kinases such as BIN2 integrate a vast number of signaling pathways and, together
1112 with receptor complexes at the cell surface, comprise a surveillance system fine-tuned to both
1113 biotic and abiotic cues (Lv & Li, 2020; Planas-Riverola *et al*, 2019; Youn & Kim, 2015; Li *et al*,
1114 2021; Song *et al*, 2023). BIN2 resides at the plasma membrane and in the cytosol and TRAPPII
1115 resides at the cytosol and in the TGN (Qi *et al*, 2011; Naramoto *et al*, 2014; Rybak *et al*, 2014;
1116 Ravikumar *et al*, 2018). We propose that, in the cytosol, the BIN2-TRAPPII interaction serves in
1117 the relay of information from the PM to the TGN. As an early endosome, the TGN is a central hub
1118 in the flow of information to and from the cell surface. It is also intimately connected to the late
1119 endosome (or the pre-vacuolar compartment) and to the Golgi. Thus, the AtSK-TRAPPII
1120 interaction would integrate all levels of cellular organization. We posit that signal integration and
1121 decision-making occur at the AtSK-TRAPPII interface and that, downstream of TRAPPII, Rab
1122 GTPase cascades are implicated in implementing decisions reached at the AtSK-TRAPPII
1123 module.
1124 In the lower panel we show one example of an adaptive growth decision in 10-day-old seedlings
1125 (Col-0 wild-type). Bar plots depict hypocotyl (green) versus root (beige-brown) lengths. Light: light
1126 grown seedling with a short hypocotyl and a long root. Dark: a seedling germinated in the dark
1127 with a long hypocotyl and a short root. DarkW: Water deprivation in the dark; the hypocotyl is
1128 shorter and the root longer than under dark conditions. The dotted green arrow (dark, darkW)
1129 represents the incentive for hypocotyl elongation in search of light and the brown arrow (darkW)
1130 the incentive for root growth in search of water. Thus, darkW is a “conflict of interest” scenario in
1131 which hypocotyl and root growth have competing interests (Kalbfuß *et al*, 2022). Figure created
1132 with BioRender.

1133 **SUPPORTING INFORMATION**

1134

1135 **Figure S1.** Selected brassinosteroid signaling components in CLUB:GFP IP-MS.

1136 **Figure S2.** Fragment ion mass spectra of AtTRS120 phosphopeptides found in TRS120:GFP
1137 IP-MS.

1138 **Figure S3.** Fragment ion mass spectra of AtSK/GSK3 kinases found in TRS120:GFP IP-MS.

1139 **Figure S4.** BIN2 phosphorylates TRS120 preferentially at the Sγ site.

1140 **Figure S5.** Pharmacological inhibition of TRAPPII phosphorylation by AtSKs *in vivo.*

1141 **Figure S6.** Cytokinesis and protein sorting in *bin2-1.*

1142 **Figure S7.** Response to additive stress: response quotients and volcano plots.

1143 **Figure S8.** Light responses in *bin2*, *trappii* and *echidna* mutants.

1144 **Figure S9.** Characterization of TRS120:GFP phosphovariants.

1145 **Figure S10.** Localization of TRS120:GFP phosphovariants.

1146 **Figure S11.** The etiolation response in TRS120 phosphovariants.

1147 **Figure S12.** Role of TRS120 phosphorylation status on adaptive growth responses under
1148 additive stress conditions.

1149 **Table S1.** Mutant lines used in this study.

1150 **Table S2.** Selected brassinosteroid signaling proteins in the CLUB interactome.

1151 **Supporting Methods.**

1152

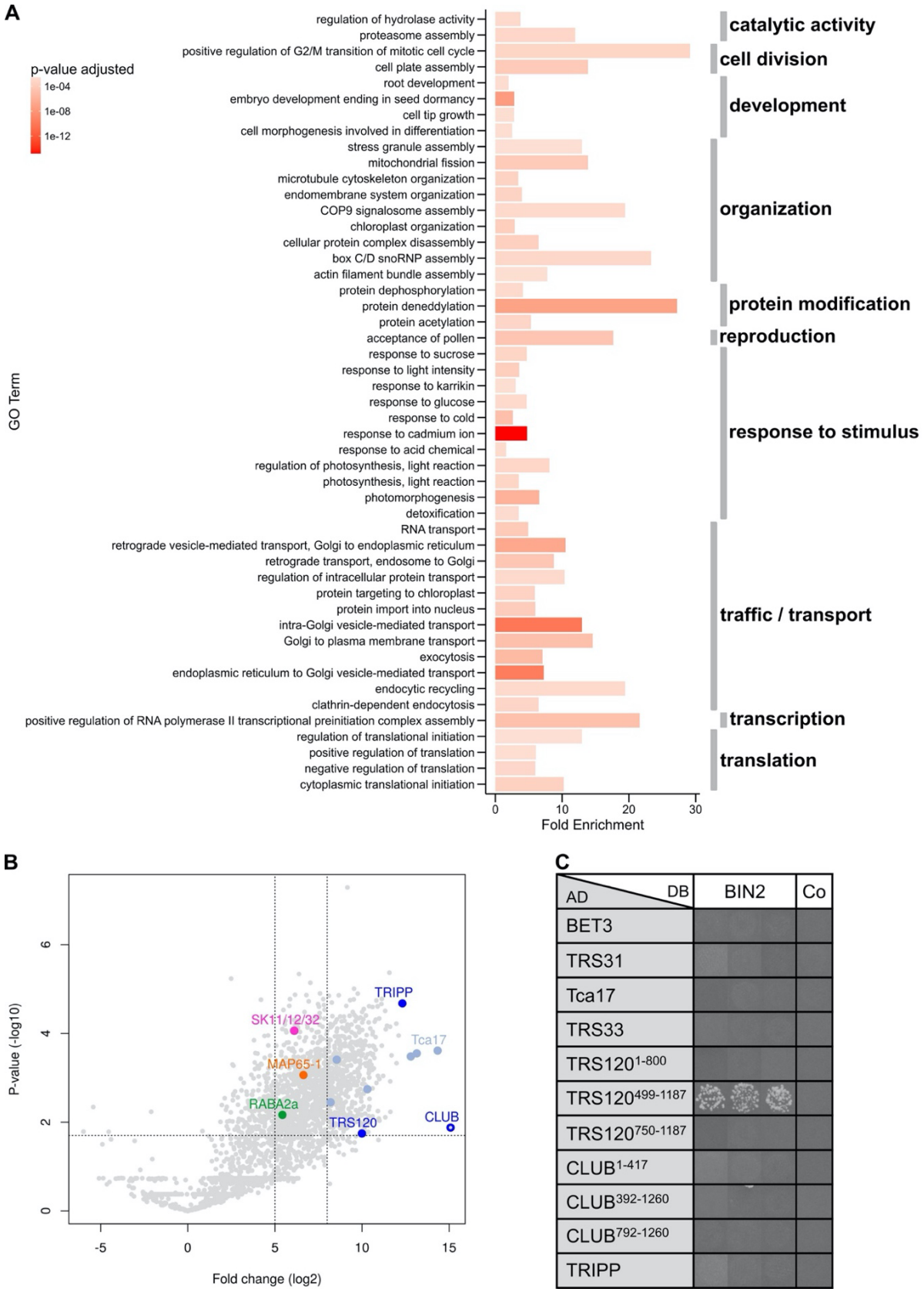

Figure 1. The TRAPPII interactome.

A. Gene ontology (GO) term enrichment analysis of the TRAPPII interactome. Depicted are fold enrichments

of GO terms of level 0 as bar plots colored by significance level. The data are derived from an analysis of IP-MS from inflorescences with the TRAPPII-specific subunit CLUB-GFP as bait (see Fig. 1B; Kalde *et al*, 2019). Terms are grouped by manually annotated super-categories. Metabolic processes were excluded for simplification. Note that the super categories organization (9) and traffic/transport (12) make up the majority of GO terms (21/49) and that response to stimulus (11) comprises the second largest category. Cutoffs were set at 1.5 for fold-change and 0.003 for the *P*-value, which was adjusted for the false discovery rate.
B. IP-MS with the TRAPPII-specific subunit CLUB-GFP as bait (Kalde *et al*, 2019). Inflorescences were used. Each protein was present in all three biological replicates. The ratio (or fold-change) was calculated for each protein as the average intensity of the signal in the experiment divided by its average intensity in the soluble GFP empty vector control. The *P*-value (depicted along a negative log10 scale) is plotted against the signal ratio. Dotted grey lines represent cutoffs: *P*-value < 0.02 and Ratio > 8 or > 5. Note that TRAPPII subunits (light blue for core TRAPP; dark blue for TRAPPII-specific subunits; the AtTRS130/CLUB-GFP TRAPPII-specific bait is depicted as an open circle) are in the upper right field, indicating high abundance and good reproducibility. AtSKs (magenta), MAP65-1 (orange) and Rab A2a GTPase (green) are all in the upper middle field; these may be transient interactors of TRAPPII. Note that AtSKs (AtSK11/12/32) are more significant than validated interactors such as MAP65 and RabA2a (Kalde *et al*, 2019; Steiner *et al*, 2016).
C. Yeast two-hybrid assays of interactions between BIN2 and TRAPPII subunits. BIN2 was fused to the GAL4 DNA-binding domain (DB) and TRAPPII subunits and truncations thereof (CLUB$^{1-417}$, CLUB$^{392-1260}$, CLUB$^{792-1260}$, TRS120$^{1-800}$, TRS120$^{499-1187}$ and TRS120$^{750-1187}$; referred to below as CLUB-C1, -C2, -C3 and TRS120-T1, -T2, -T3) to the GAL4 activation domain (AD). As negative control, the BIN2-DB construct was tested with the empty AD vector. Interactions were verified by pairwise one-on-one mating in four independent replicate experiments. The panels are from different plates. The results show interactions between BIN2 and AtTRS120$^{499-1187}$ wild-type. BIN2 bound specifically to the TRAPPII subunit TRS120 (TRS120$^{499-1187}$ / T2 truncation) and not with other TRAPPII subunits or truncations. In a total of > 2400 pairwise tests, BIN2 was the only kinase we found that interacted with a TRAPP subunit. The Y2H did not detect AtTRS130/CLUB-BIN2 interaction shown in Fig. 1B, which shows co-purified proteins that can include indirect - as opposed to binary - interactors. Related to Fig. S1.

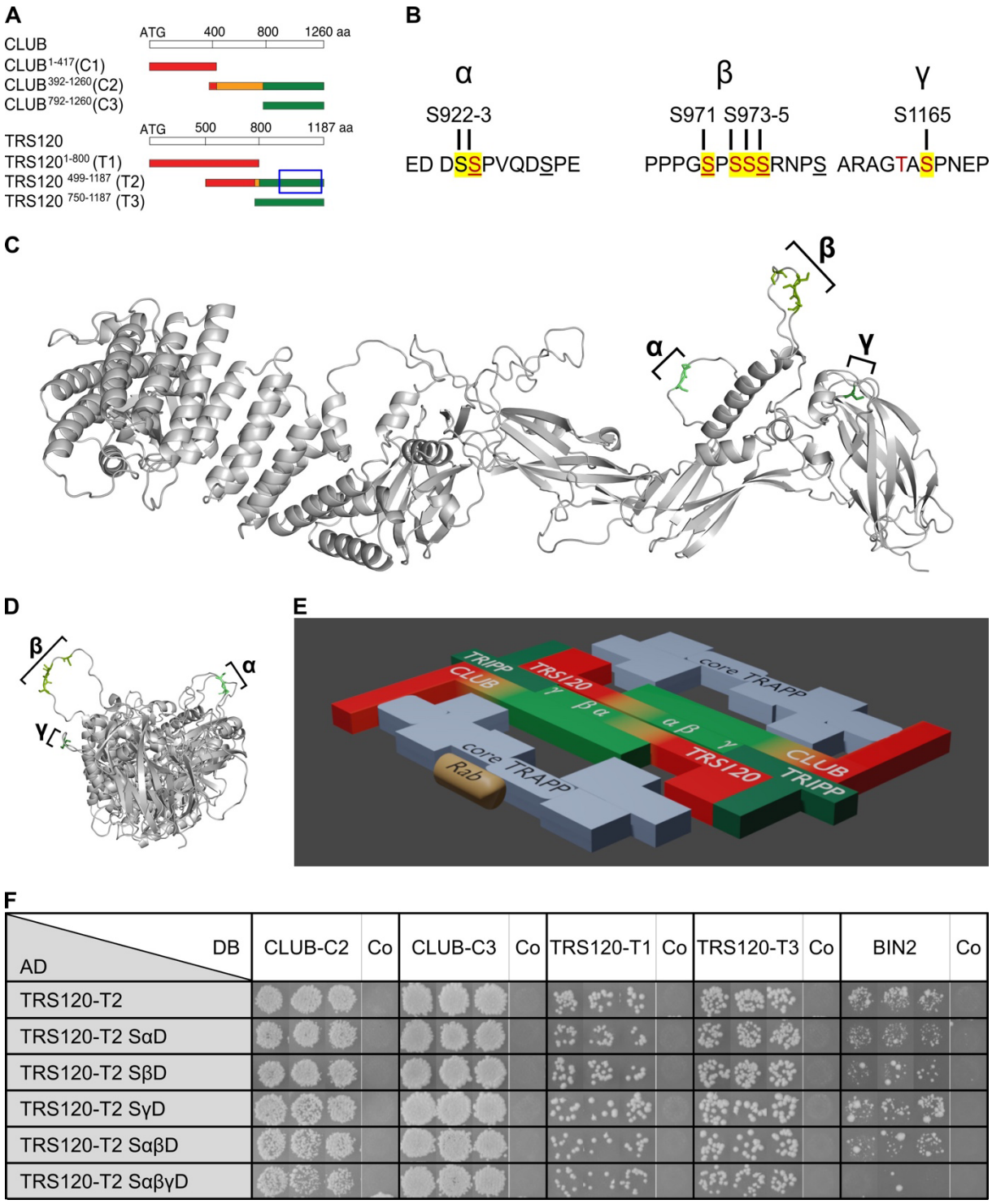

Figure 2. GSK3/AtSK sites in TRAPPII and binary interactions.

A. TRAPPII-specific truncations for yeast two-hybrid were based on phylogenetic analysis (Steiner *et al*, 2016). Conserved sequences are depicted in red, intermediate degrees of conservation in orange, and plant-specific sequences are in green. All three GSK3 sites found to be phosphorylated *in vivo* (delineated by a blue rectangle) reside in the plant-specific moiety of TRS120-T2 (green).

B. GSK3 sites in TRS120-T2. The α-phosphosite of AtTRS120 spans amino acid positions S922 and S923, the β-phosphosite amino acids S971-S975 and the γ-phosphosite amino acid residue S1165. The canonical GSK3 consensus sequence is: (pS/pT)*XXX*(S/T), and the β-phosphosite fits this definition (see underlined

SXXXS). Even though they are annotated as GSK3 sites in the PPSP (https://www.phosphosite.org) database, the α-phosphosite deviates somewhat with SXXXXS, and the γ-phosphosite deviates completely. Amino acids in red were mutated to A or D via site-directed mutagenesis. Amino acids highlighted in yellow were found to be phosphorylated *in vivo* and these were all serines (see Fig. S2).
C, D. Mapping of GSK3/AtSK sites on an Alphafold structural prediction (Jumper *et al*, 2021; Varadi *et al*, 2022) of AtTRS120. A lateral view (C) and a frontal perspective (D) are shown. Note that all three GSK3/AtSK sites reside in unstructured, flexible and accessible regions of the protein.
E. The Arabidopsis TRAPPII complex consists of six shared core subunits (light blue) and three TRAPPII-specific subunits (CLUB/AtTRS130, AtTRS120 and the plant-specific subunit TRIPP), and forms a dimer with plant-specific domains (green) at the predicted dimer interface (Garcia *et al*, 2020; Kalde *et al*, 2019). A Rab-GTPase (beige) is shown to bind core-TRAPP subunits at the approximate location of the putative GEF catalytic site, based on yeast models (Cai *et al*, 2008; Thomas *et al*, 2019).
F. Yeast two-hybrid assays of interactions between BIN2 and TRAPPII truncations (CLUB-C2, CLUB-C3, TRS120-T1, TRS120-T3), as positive controls, fused to the GAL4 DNA-binding domain (DB) and TRS120-T2 truncation and its phosphomutants TRS120-T2 SαD, SβD, SγD, SαβD and SαβγD fused to the GAL4 activation domain (AD). As negative control, the BIN2-DB construct was tested with the empty AD vector. Interactions were verified by pairwise one-on-one mating in four independent replicate experiments; for the control (Co) only one representative example is shown. The panels are from different plates. The results show interactions between BIN2 and AtTRS120-T2 wild-type and phosphovariants; there was, however, no reproducible interaction if all three target sites were phosphomimetic. Related to Fig. S1-S5.

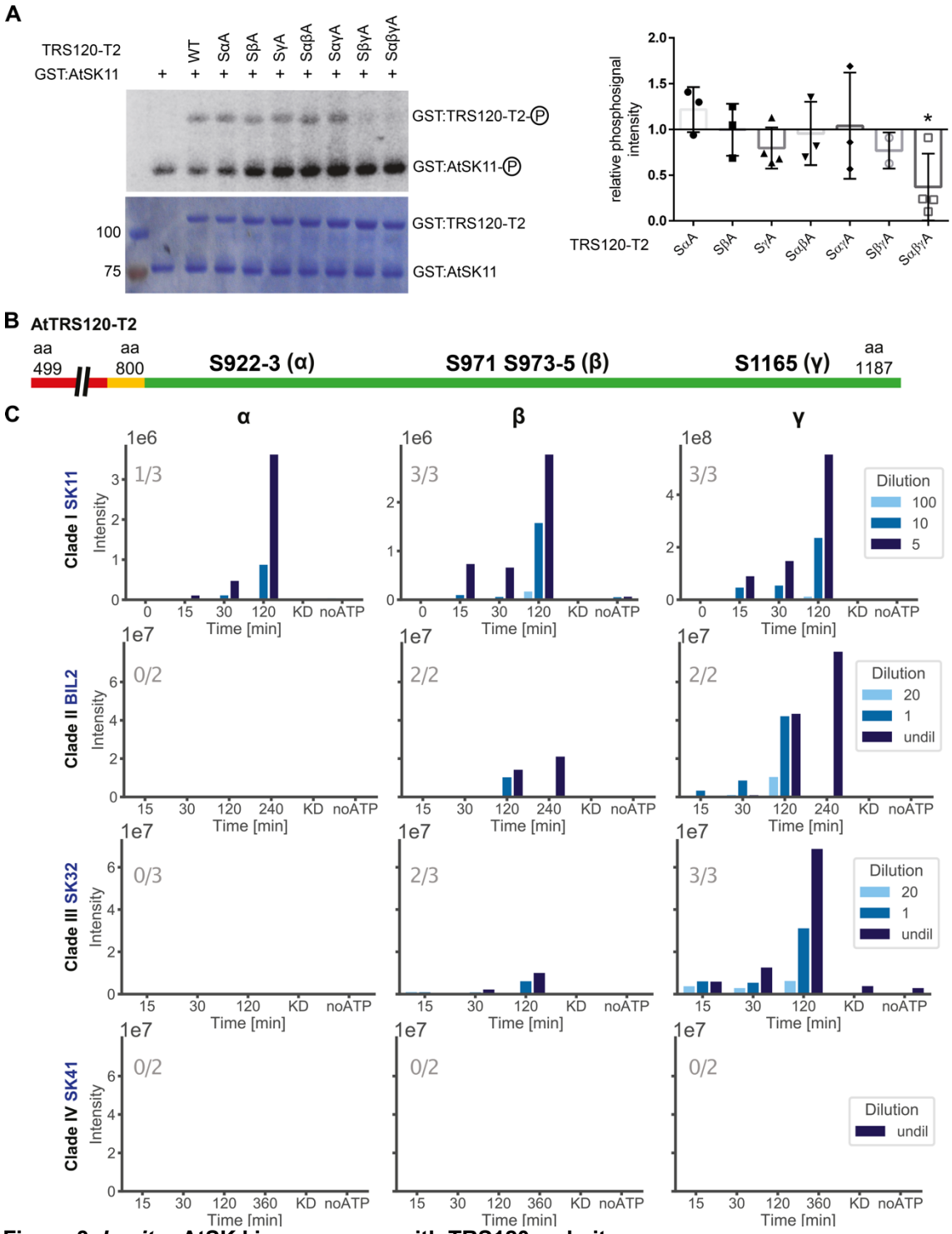

Figure 3. *In vitro* AtSK kinase assays with TRS120 as bait.

A. *In vitro* kinase assays using GST:AtSK11 (72 kDa) and GST:TRS120-T2 (100 kDa). The change of phosphosignal is shown in a representative autoradiograph (upper panel) and the loaded protein amount in the corresponding CBB (lower panel). Non-phosphorylated variants were used as negative controls. The means ±SD of phosphosignals were normalized to the protein amount; nonmutated TRS120-T2 WT is set at 1.0 (right panel); n = 3 independent experiments; *: P<0.05 paired two-sided student's t-test; TRS120-T2-SαβγA versus TRS120-T2 WT).

B. AtTRS120-T2 has highly (red) and moderately (orange) conserved sequences, as well as plant-specific sequences (green). Three GSK3 sites (referred to as α, β, γ; see Fig. 2B) can be found in the plant-specific T2 domain.
C. Kinase assays were performed *in vitro* with mass-spectrometry readout. One member of each shaggy-like kinase clade (AtSKs; see Fig. S3A) was used with the TRS120-T2 truncation as substrate. Dilution series are depicted in different shades of blue. AtSKs in clades I-III differentially phosphorylate the substrate at three GSK3 consensus sites (with a preference for the γ site) in a time-dependent and concentration-dependent manner. A clade IV AtSK did not phosphorylate at all. Samples incubated for 120 min in a kinase buffer without ATP, or samples in which the kinase was heat inactivated, served as negative controls. The numbers in grey in each plot denote the number of times the phosphorylation event was seen in the given number of independent replicates. Note the higher intensity of the TRS120-γ peptide, especially for Clade I/SK11 (1e8 for TRS120-γ versus 1e6 for TRS120-α and TRS120-β on the Y axis). Related to Fig. S1-S6.

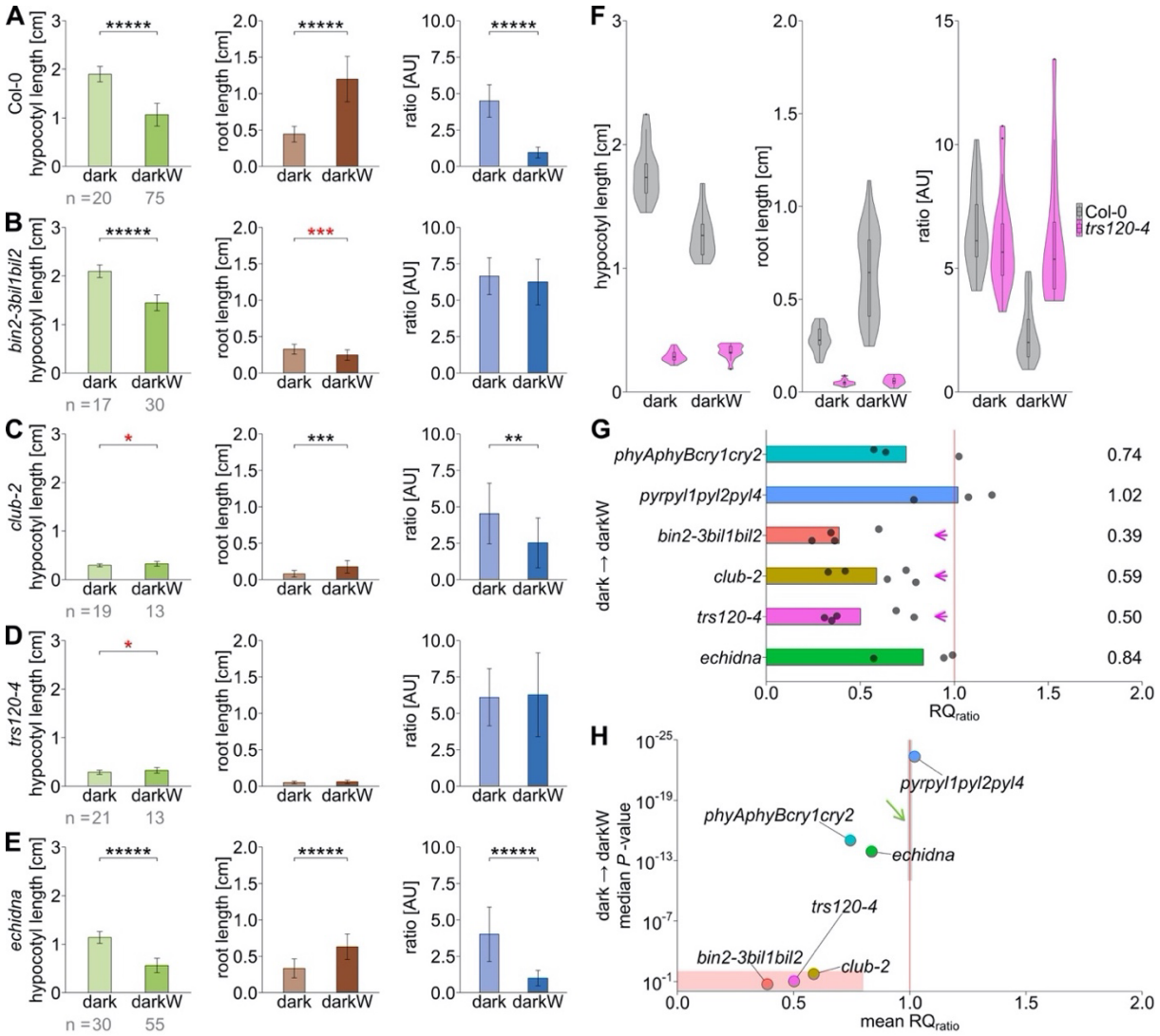

Figure 4. Role of the TRAPPII complex versus ECHIDNA in hypocotyl/root tradeoffs.
Seedlings were germinated on ½ MS in the dark (dark) or in dark with -0.4MPa water stress (darkW). **A.** Col-0 (wild-type). **B.** BR signaling mutant *bin2-3bil1bil2* triple knockout (from Kalbfuß *et al*, 2022). **C.** *club-2*, a null *trappii* mutant. **D.** *trs120-4*, a null *trappii* allele. **E.** *echidna* null allele, impaired in TGN structure and function. At least 3 experiments were performed for each line, and a representative one is shown here on the basis of RQ and *P*-values. **F.** Violin plot for a direct comparison between *trs120-4* and the corresponding wild-type (Col-0; in the same experiment and on the same PEG plates) showing that the response to a shift from dark to darkW seen in the wild-type was not observed in *trs120-4*. **G.** Normalized response quotient RQ_{ratio}. Each replicate is represented by a dot. Note that the triple *bin2-3bil1bil2* knock out, *trs120-4* and *club-2* had attenuated responses (magenta arrows). **H.** Volcano plot with the mean RQ_{ratio} depicted on the X axis and the median *P*-value of the response on the Y axis (negative log scale; a median of all replicates was used). The area shaded in grey on the red line (green arrow) is where wild-type ecotypes would theoretically map onto the plot. Mutants in the lower left quadrant (peach shading) were considered to have a "confused decision phenotype" (see text). *trs120-4* mutants mapped to the lower left quadrant and qualified as decision mutants on two counts: (i) a consistently opposite hypocotyl response (red asterisk in D), (ii) failure to adjust the hypocotyl/root ratio to darkW (the ratio for darkW is the same as for dark in panel D), translating into a non-significant *P*-value for the ratio response (H). The number (n) of seedlings measured per condition is in grey below the mean ±SD bar graphs. *P*-values were computed with a two-tailed student's t-test and are represented as follows: *: P<0.05; **: P<0.01; ***: P<0.001; ****: P<0.0001; *****: P<0.00001. Mutant alleles and the corresponding ecotypes are described in Table S1. See related Fig. S7.

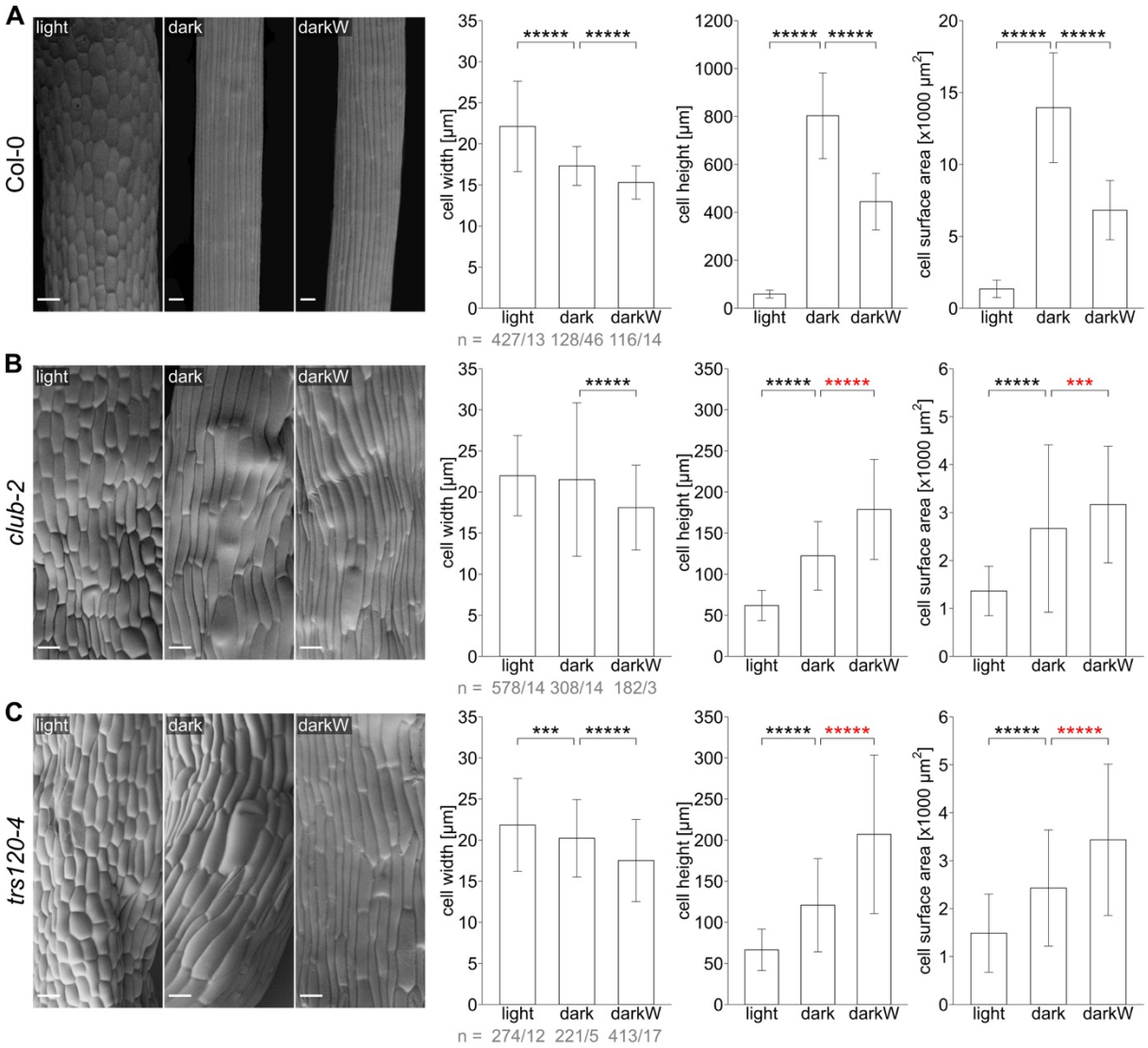

Figure 5. Cell elongation in *trappii* hypocotyls under additive stress.

A. Col-0 wild-type.

B. *club-2,* null *trappii* allele.

C. *trs120-4,* null *trappii* allele.

Seedlings were germinated in the light, or in the dark with (darkW) or without (dark) water stress (PEG - 0.4MPa). The cellular growth parameters width and height were measured based on SEM images. The cell surface area was calculated as the product of cell width and heigth. The *trappii* mutants, *club-2* and *trs120-4*, showed the opposite hypocotyl cell height and cell surface adaptations to dark-to-darkW conditions (red asterisks in B and C) than the wild-type control. Representative SEM images of seedlings grown under the specified conditions are shown (scalebar = 20 µm). The sample size (n) is given as the number of cells/ number of seedlings that were analyzed in grey below the graph. Shown are means ±SD. *P*-values were computed with a two-tailed student's t-test and are represented as follows: ***: P<0.001; ****: P<0.0001; *****: P<0.00001.

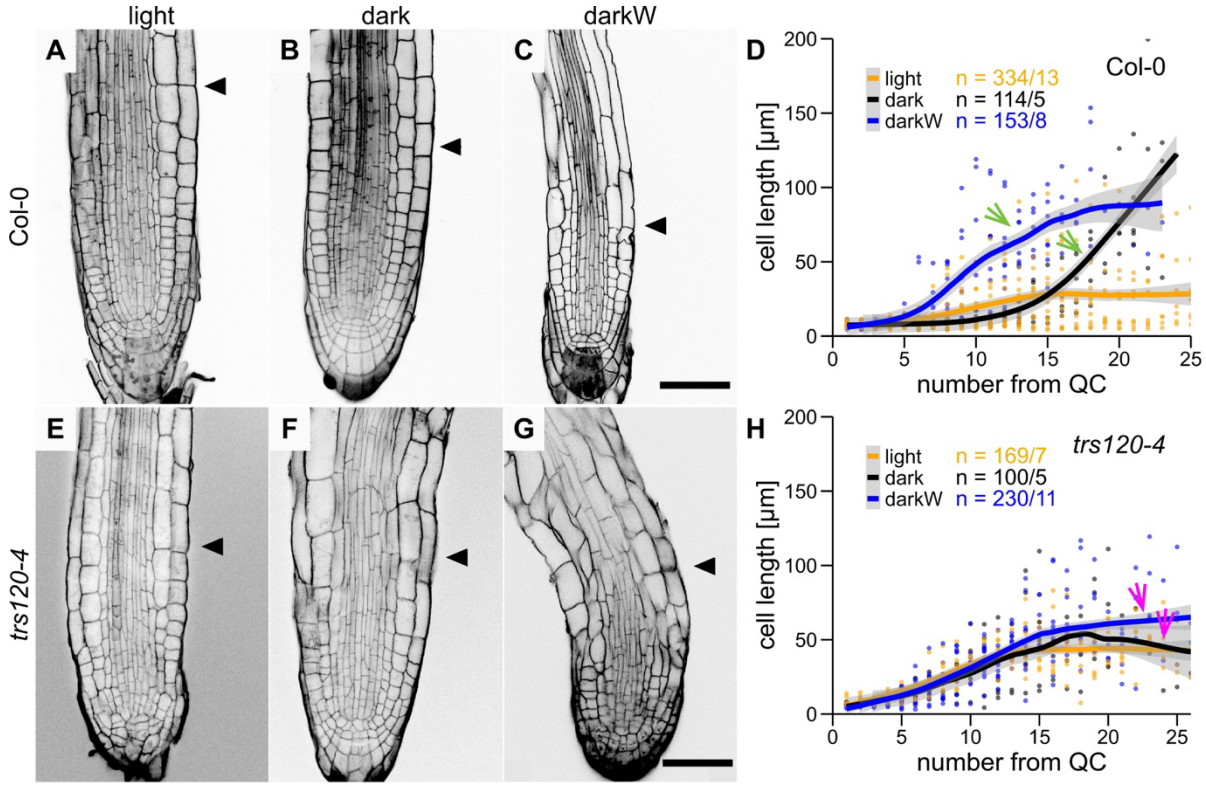

Figure 6. Root meristem properties of *trappii* mutants under single versus additive stress conditions. Seedlings were grown in the light (orange), dark (black) or dark with -0.4MPa water stress (darkW; blue).

A-D. Col-0 wild-type.

E-H. *trs120-4* null mutant.

(A-C) and (E-G) confocal micrographs of mPS-PI stained root tips under different environmental conditions; black arrows mark the junction between the meristematic and elongation zones.

D, H. 10 days after incubation, the cell lengths were measured in single cortex cell files, starting at the cortex/endodermis initials. The fitted lines were generated with Local Polynomial Regression Fitting with the 'loess' method in R; grey shading designates the 95 percent confidence interval. Cell lengths of consecutive cells as a function of cell number from the quiescent centre (QC); the green arrows point to the steep slope under the dark condition and steeper slope under darkW condition - the initiation of elongation - in the wild-type (D); magenta arrows point to flatter, unadjusted slopes under dark versus darkW in *trappii* (*trs120-4*) mutants (H). The sample size (n) is given as the number of cells/ number of seedlings that were analyzed in panels (D,H). Scale bar is 50 µm.

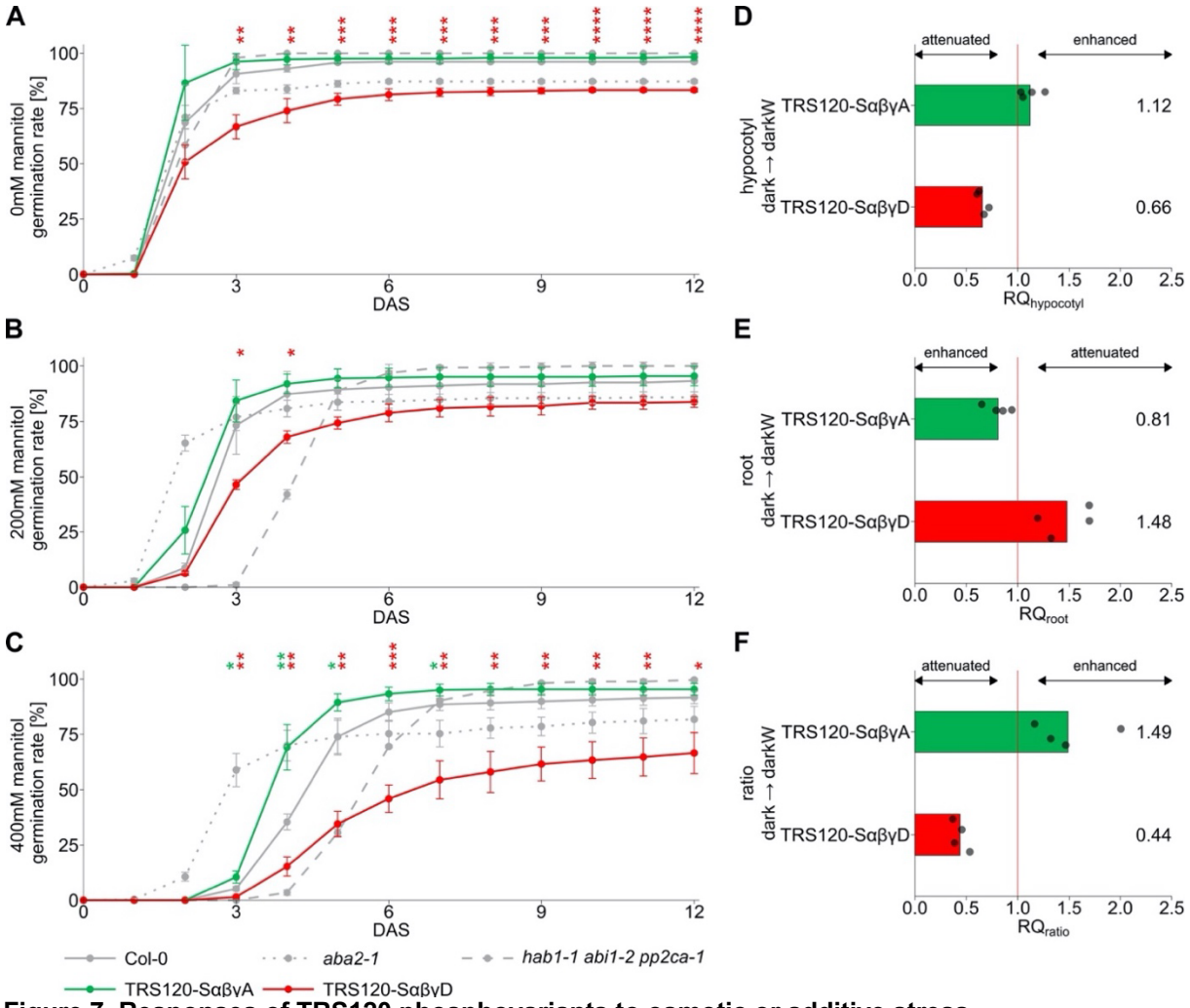

Figure 7. Responses of TRS120 phosphovariants to osmotic or additive stress.

Phosphovariants of P_{TRS120}::TRS120-GFP (Rybak *et al*, 2014) were in *trs120-4* homozygous backgrounds with the exception of the TRS120-SαβγD variant in panels A-C, which was in a hemizygous *trs120-4*/+ background.

A-C. Germination of TRS120 phosphovariants under osmotic stress**.** Effect of A) 0 mM, B) 200 mM and C) 400 mM mannitol on seed germination of the TRS120-SαβγA, the TRS120-SαβγD mutants and the following controls: Col-0 wild-type; the ABA deficient mutant *aba2-1* and the ABA PP2C co receptor triple knock-out line *hab1-1 abi1-2 pp2ca-1*. The non-phosphorylatable TRS120-SαβγA mutation increased seed germination on higher mannitol concentrations, whereas the phosphomimetic TRS120-SαβγD decreased seed germination. Shown are the means ± SD of three technical replicates. Similar results were obtained in three independent biological replicates. Stars indicate statistical significance compared to the wild-type Col-0 calculated with a two-tailed student's t-test (*: P<0.05; **: P<0.01; ***: P<0.001; ****: P<0.0001; *****: P<0.00001). DAS: days after stratification.

D-F. Response quotients (RQ) of A) the hypocotyl, B) the root and C) the hypocotyl/root ratio of the non-phosphorylatable TRS120-SαβγA and the phosphomimetic TRS120-SαβγD mutants for dark-to-dark with water stress (-0.4MPa, darkW) adaptation. The divergent hypocotyl and root responses of TRS120-SαβγA and TRS120-SαβγD mutants resulted in a strong hypocotyl/root ratio phenotype under darkW conditions compared to the TRS120-WT control. TRS120-SαβγA showed an enhanced ratio adaption, whereas TRS120-SαβγD mutants had an attenuated ratio response. RQ response quotients are normalized to the rescue mutant TRS120-WT (P_{TRS120}::TRS120-GFP in *trs120-4/trs120-4*). A value of 1 (vertical red line) corresponds to an identical adaptation to darkW conditions as the rescue mutant. Dots represent biological replicates, of which there were a total of four primary transformants per line. Mean RQ values are given on the right.

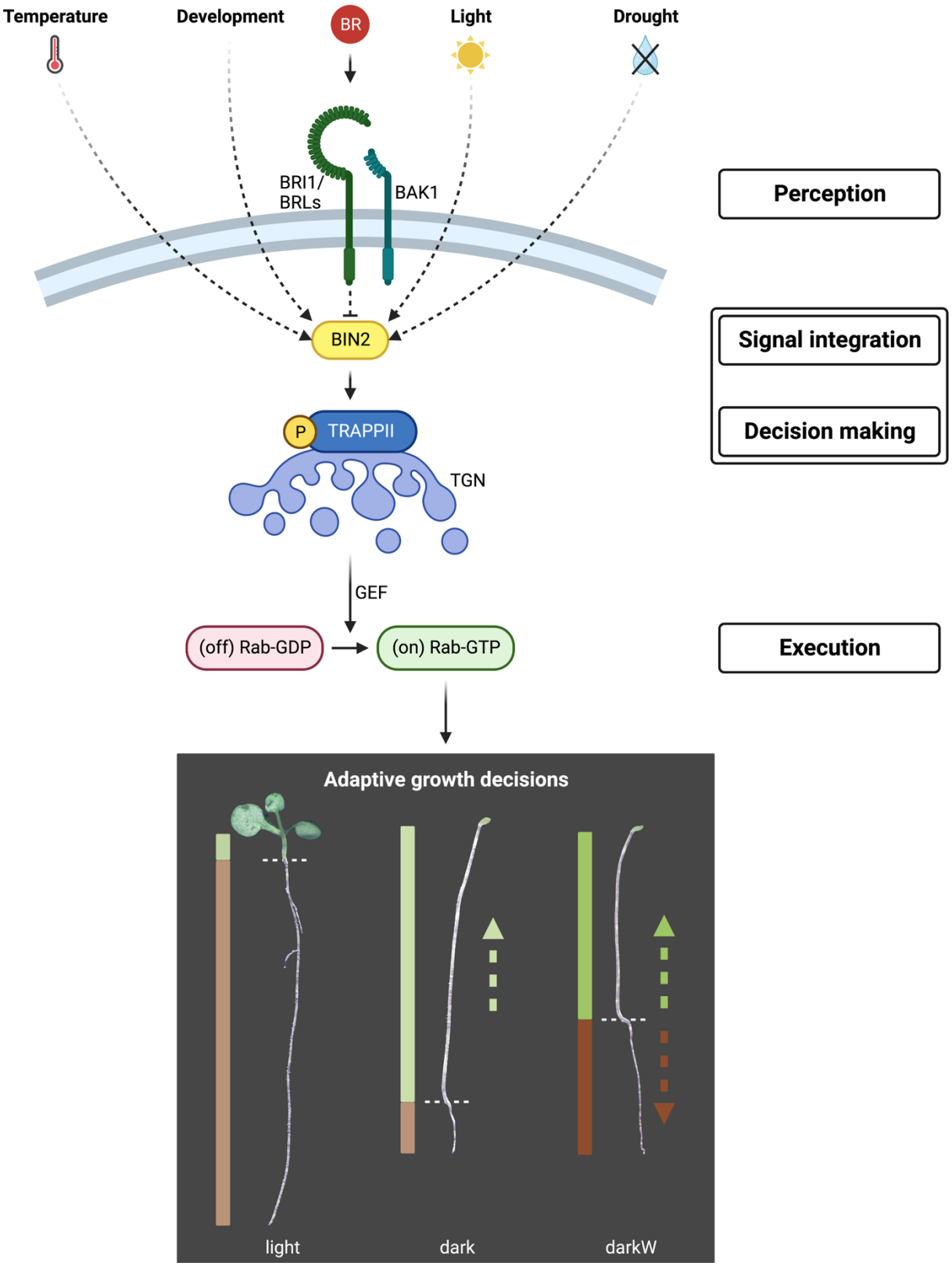

Figure 8. Flow diagram suggesting how BIN2 might mediate plant adaptive responses by phosphorylating the TRAPPII complex.
Shaggy-like kinases such as BIN2 integrate a vast number of signaling pathways and, together with receptor complexes at the cell surface, comprise a surveillance system fine-tuned to both biotic and abiotic cues (Lv

& Li, 2020; Planas-Riverola *et al*, 2019; Youn & Kim, 2015; Li *et al*, 2021; Song *et al*, 2023). BIN2 resides at the plasma membrane and in the cytosol and TRAPPII resides at the cytosol and in the TGN (Qi *et al*, 2011; Naramoto *et al*, 2014; Rybak *et al*, 2014; Ravikumar *et al*, 2018). We propose that, in the cytosol, the BIN2-TRAPPII interaction serves in the relay of information from the PM to the TGN. As an early endosome, the TGN is a central hub in the flow of information to and from the cell surface. It is also intimately connected to the late endosome (or the pre-vacuolar compartment) and to the Golgi. Thus, the AtSK-TRAPPII interaction would integrate all levels of cellular organization. We posit that signal integration and decision-making occur at the AtSK-TRAPPII interface and that, downstream of TRAPPII, Rab GTPase cascades are implicated in implementing decisions reached at the AtSK-TRAPPII module.
In the lower panel we show one example of an adaptive growth decision in 10-day-old seedlings (Col-0 wild-type). Bar plots depict hypocotyl (green) versus root (beige-brown) lengths. Light: light grown seedling with a short hypocotyl and a long root. Dark: a seedling germinated in the dark with a long hypocotyl and a short root. DarkW: Water deprivation in the dark; the hypocotyl is shorter and the root longer than under dark conditions. The dotted green arrow (dark, darkW) represents the incentive for hypocotyl elongation in search of light and the brown arrow (darkW) the incentive for root growth in search of water. Thus, darkW is a “conflict of interest” scenario in which hypocotyl and root growth have competing interests (Kalbfuß *et al*, 2022). Figure created with BioRender.